

# Double Trouble in Double Descent: Bias and Variance(s) in the Lazy Regime

Stéphane d’Ascoli\*, Maria Refinetti\*, Giulio Biroli and Florent Krzakala

Laboratoire de Physique de l’Ecole Normale Supérieure, Université PSL,  
CNRS, Sorbonne Université, F-75005 Paris, France

\* Equal contribution.

## Abstract

Deep neural networks can achieve remarkable generalization performances while interpolating the training data perfectly. Rather than the U-curve emblematic of the bias-variance trade-off, their test error often follows a “double descent”—a mark of the beneficial role of overparametrization. In this work, we develop a quantitative theory for this phenomenon in the so-called lazy learning regime of neural networks, by considering the problem of learning a high-dimensional function with random features regression. We obtain a precise asymptotic expression for the bias-variance decomposition of the test error, and show that the bias displays a phase transition at the interpolation threshold, beyond it which it remains constant. We disentangle the variances stemming from the sampling of the dataset, from the additive noise corrupting the labels, and from the initialization of the weights. Following Geiger et al. [1] we first show that the latter two contributions are the crux of the double descent: they lead to the overfitting peak at the interpolation threshold and to the decay of the test error upon overparametrization. We then quantify how they are suppressed by ensembling the outputs of  $K$  independently initialized estimators. For  $K \rightarrow \infty$ , the test error remains constant beyond the interpolation threshold. We further compare the effects of overparametrizing, ensembling and regularizing. Finally, we present numerical experiments on classic deep learning setups to show that our results hold qualitatively in realistic lazy learning scenarios.

Correspondence: [stephane.dascoli@ens.fr](mailto:stephane.dascoli@ens.fr), [maria.refinetti@ens.fr](mailto:maria.refinetti@ens.fr).

## 1 Introduction

Deep neural networks have achieved breakthroughs in a plethora of contexts, such as image classification [2, 3], speech recognition [4], and automatic translation [5]. Yet, theory lags far behind practice, and the key reasons underpinning the success of deep learning remain to be clarified.

One of the main puzzles is to understand the excellent generalization performance of heavily overparametrized deep neural networks able to fit random labels [6]. Such *interpolating* estimators—that can reach zero training error—have attracted a growing amount of theoretical attention in the last few years, see e.g. [7, 8, 9, 10, 11]. Indeed, classical learning theory suggests that generalization should first improve then worsen when increasing model complexity, following a U-shape curve characteristic of the bias-variance trade-off. Instead, deep neural networks [12, 13, 14] as well as other machine learning models [8], follow a different curve, coined *double descent*.

This curve displays two regimes : the *classical* U-curve is superseded at high complexity by a *modern* interpolating regime where the test error decreases monotonically with overparametrization [15]. Between these two regimes, i.e. at the *interpolation threshold* where training error vanishes, a *peak* occurs in absence of regularization, sometimes called the *jammed* peak [13] due to similarities with a well-studied phenomenon in the Statistical Physics literature [16, 17, 18, 19, 20, 21]. The reasons behind the performance of deep neural networks in the overparametrized regime are still poorly understood, even though some mechanisms are known to play an important role, such as the implicit regularization of stochastic gradient descent which allows to converge to the minimum norm solution, and the convergence to mean-field limits [22, 7, 23, 24, 25].

Here we present a detailed investigation of the double descent phenomenon, and its theoretical explanation in terms of bias and variance in the so-called *lazy* regime [23]. This theoretically appealing scenario, where the weights stay close to their initial value during training, is called *lazy learning* as opposed to *feature learning* where the weights change enough to learn relevant features [23, 26, 27]. Although replacing learnt features by random features may appear as a crude simplification, empirical results show that the loss in performance can be rather small in some cases [28, 24]. A burst of recent papers showed that in this regime, neural networks

behave like kernel methods [29, 30, 31] or equivalently random projection methods [32, 23, 24]. This mapping makes the training analytically tractable, allowing, for example, to prove convergence to zero error solutions in overparametrized settings.

Optimization plays an important role in neural networks, and in particular for the double descent phenomenon, by inducing implicit regularization [33] and fluctuations of the learnt estimator [1]. Disentangling the variance stemming from the randomness of the optimization process from that the variance due to the randomness of the dataset is a crucial step towards a unified picture, as suggested in [9]. In this paper, we address this issue and attempt to reconcile the behavior of bias and variance with the double descent phenomenon by providing a precise and quantitative theory in the *lazy* regime.

**Contributions** We focus on an analytically solvable model of random features (RF), introduced by [32], that can be viewed either as a randomized approximation to kernel ridge regression, or as a two-layer neural network whose first layer contains fixed random weights. The latter provides a simple model for lazy learning. Indeed, suppose that a neural network learns a function  $f_\theta(\mathbf{x})$  that relates labels (or responses)  $y$  to inputs  $\mathbf{x}$  via a set of weights  $\theta$ . The lazy regime is defined as the setting where the model can be linearized around the initial conditions  $\theta_0$ . Assuming that the initialization is such that  $f_{\theta_0} \approx 0$ <sup>1</sup>, one obtains:

$$f_\theta(\mathbf{x}) \approx \nabla_\theta f_\theta(\mathbf{x})|_{\theta=\theta_0} \cdot (\theta - \theta_0). \quad (1)$$

In other words, the lazy regime corresponds to a linear fitting problem with a random feature vector  $\nabla_\theta f_\theta(\mathbf{x})|_{\theta=\theta_0}$ . In this setting our contributions are:

- We demonstrate how to disentangle quantitatively the contributions to the test error of the bias and the various sources of variance of the estimator, stemming from the sampling of the dataset, from the additive noise corrupting the labels, and from the initialization of the random feature vectors.
- We give a sharp asymptotic formula for the effect of *ensembling* (averaging the predictions of indepently initialized estimators) on these various terms. We show in particular how the over-fitting peak at the interpolation threshold can be attenuated by ensembling, as observed in real neural networks [1]. We also compare the effect of ensembling, overparametrizing and optimally regularizing.
- Several conclusions stem from the above analysis. First, the over-fitting near the interpolation threshold is entirely due to the variances due to the additive noise in the ground truth and the initialization of the random features. Second, the data sampling variance and the bias both display a phase transition at the interpolation threshold, and remain constant in the overparametrized regime. Hence, the benefit of ensembling and overparametrization beyond the interpolation threshold is solely due to a reduction of the noise and initialization variances.

Finally, we present numerical results on a classic deep learning scenario in the lazy learning regime to show that our findings, obtained for simple random features and i.i.d. data, are relevant to realistic setups involving correlated random features and realistic data.

The analytical results we present are obtained using a heuristic method from Statistical Physics called the Replica Method [34], which despite being non-rigorous has shown its remarkable efficacy in many machine learning problems [35, 18, 36, 37] and random matrix topics, see e.g. [38, 39, 40]. While it is an open problem to provide a rigorous proof of our computations, we check through numerical simulations that our asymptotic predictions are extremely accurate at moderately small sizes.

**Related work** Our work crucially builds on the two recent contributions by Geiger *et al.* [1], and Mei and Montanari [11]. The authors of [1] carried out a series of experiments in order to shed light on the generalization properties of neural networks. The current work is inspired by their observations and scaling theory about the role of the variance due to the random initialization of the weights in the double-descent curve. They argued that the decrease of the test error in the limit of very wide networks is due to this source of variance, which vanishes inversely proportional to the width of the network. They then used ensembling to empirically support these findings in more realistic situations. Another related work is [9], which disentangles the various sources of variance in the process of training deep neural networks. On the analytical side, our paper builds on the results of [11], which provide a precise expression of the test error of the RF model in the high-dimensional limit where the number of random features, the dimension of the input data and the number of data points are sent to infinity with their relative ratios fixed. The double descent was also studied analytically for various types of linear models, both for regression [7, 10, 41, 42] and classification [43, 44, 45]. An example of a practical method

<sup>1</sup>One can alternatively define the estimator as  $f_\theta - f_{\theta_0}$  [23].

that uses ensembling in kernel methods is detailed in [46]. Note that this work performs an average over the sampling of the random feature vectors in contrast to [47] where the average is taken over the sampling of the data set.

**Reproducibility** The codes necessary to reproduce the results presented in this paper and obtain new ones are given at [https://github.com/mariaref/Random\\_Features.git](https://github.com/mariaref/Random_Features.git).

## 2 Model

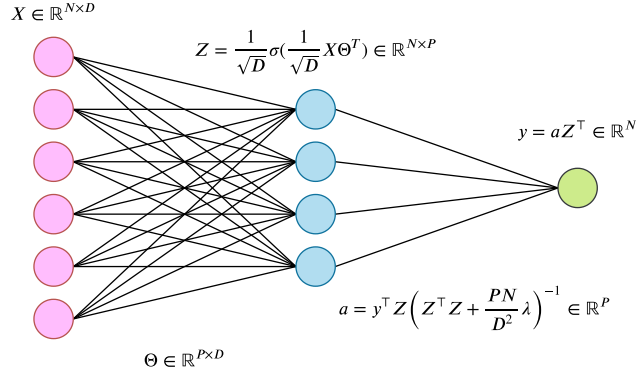


Figure 1: Illustration of a Random Feature (RF) network. The first layer weights are fixed and initialized as i.i.d. centered Gaussian variables of unit variance. The second layer weights are trained via ridge regression.

This work is centered around the RF model first introduced in [32]. Although simpler settings such as linear regression display the double descent phenomenology [10], this model is more appealing in several ways. First, the presence of two layers allows to freely disentangle the dimensionality of the input data from the number of parameters of the model. Second, it closely relates to the lazy regime of neural networks, as described above. Third, and most importantly for our specific study, the randomness of the fixed first layer weights mimics the randomness due to weight initialization in neural networks.

The RF model can be seen as a two-layer neural network whose first layer contains fixed random weights<sup>2</sup> (see figure 1):

$$\hat{f}(\mathbf{x}) = \frac{1}{\sqrt{D}} \sum_{i=1}^P \mathbf{a}_i \sigma \left( \frac{\langle \boldsymbol{\theta}_i, \mathbf{x} \rangle}{\sqrt{D}} \right). \quad (2)$$

In the above,  $\boldsymbol{\theta}_i$  is the  $i^{\text{th}}$  random feature vector, i.e the  $i^{\text{th}}$  column of the random feature matrix  $\boldsymbol{\Theta} \in \mathbb{R}^{P \times D}$  whose elements are drawn i.i.d from  $\mathcal{N}(0, 1)$ .  $\sigma$  is a pointwise activation function, which we will take to be  $\text{ReLU} : x \mapsto \max(0, x)$ .

The training data is collected in a matrix  $\mathbf{X} \in \mathbb{R}^{N \times D}$  whose elements are drawn i.i.d from  $\mathcal{N}(0, 1)$ . We assume that the labels are given by a linear ground truth corrupted by some additive Gaussian noise:

$$y_\mu = \langle \boldsymbol{\beta}, \mathbf{X}_\mu \rangle + \epsilon_\mu, \quad \|\boldsymbol{\beta}\| = F, \quad \epsilon_\mu \sim \mathcal{N}(0, \tau), \quad (3)$$

$$\text{SNR} = F/\tau.$$

The generalization to non-linear functions can also be performed as in [11].

The second layer weights, i.e the elements of  $\mathbf{a}$ , are calculated by the means of ridge regression:

$$\mathcal{L}_{\text{RF}}(\mathbf{a}) \equiv \frac{1}{N} \sum_{\mu=1}^N \left( y_\mu - \sum_{i=1}^P \mathbf{a}_i \sigma \left( \frac{\langle \boldsymbol{\theta}_i, \mathbf{X}_\mu \rangle}{\sqrt{D}} \right) \right)^2 + \frac{P\lambda}{D} \|\mathbf{a}\|_2^2, \quad (4)$$

$$\hat{\mathbf{a}} \equiv \arg \min_{\mathbf{a} \in \mathbb{R}^P} \mathcal{L}_{\text{RF}}(\mathbf{a}).$$

<sup>2</sup>Note the closeness between the RF model and the "hidden manifold model" introduced in [48]. The task studied here can be seen as a linear regression task on a structured data set  $\mathbf{Z} \in \mathbb{R}^P$ , obtained by projecting the original latent features  $\mathbf{X} \in \mathbb{R}^D$ . The difference here is that the dimension of the latent space, denoted as  $D$  here, is sent to infinity together with the dimension of the ambient space.

Note that as  $P \rightarrow \infty$ , this is equivalent to kernel ridge regression with respect to the following kernel:

$$K(\mathbf{x}, \mathbf{x}') = \mathbb{E}_{\boldsymbol{\theta} \sim \mathcal{P}} \left[ \sigma(\langle \mathbf{x}, \boldsymbol{\theta} \rangle / \sqrt{D}) \sigma(\langle \mathbf{x}', \boldsymbol{\theta} \rangle / \sqrt{D}) \right],$$

where  $\mathcal{P} = \text{Unif}(\mathbb{S}^{D-1}(\sqrt{D}))$ .

The key quantity of interest is the *test error* of this model, defined as the mean square error evaluated on a fresh sample  $\mathbf{x} \sim \mathcal{N}(0, 1)$  corrupted by a new noise  $\tilde{\epsilon}$ :

$$\mathcal{R}_{\text{RF}} = \mathbb{E}_{\mathbf{x}} \left[ \left( \langle \boldsymbol{\beta}, \mathbf{x} \rangle + \tilde{\epsilon} - \hat{f}(\mathbf{x}) \right)^2 \right], \quad \tilde{\epsilon} \sim \mathcal{N}(0, \tilde{\tau}). \quad (5)$$

### 3 Analytical results

In this section, we present our main result, which is an analytical expression for the terms appearing in the decomposition of the test error.

**Decomposition of the test error** The test error can be decomposed into its bias and variance components:

$$\mathbb{E}_{\boldsymbol{\Theta}, \mathbf{X}, \boldsymbol{\epsilon}} [\mathcal{R}_{\text{RF}}] = \mathcal{E}_{\text{Noise}} + \mathcal{E}_{\text{Init}} + \mathcal{E}_{\text{Samp}} + \mathcal{E}_{\text{Bias}} + \tilde{\tau}^2. \quad (6)$$

The first three terms contribute to the variance, the fourth is the bias, and the final term  $\tilde{\tau}^2$  is simply the Bayes error. It does not play any role and will be set to zero in the rest of the paper: the only reason it was included is to avoid confusion with  $\mathcal{E}_{\text{Noise}}$  defined below.

**Noise variance:** The first term is the variance associated with the additive noise corrupting the labels of the dataset which is learnt,  $\boldsymbol{\epsilon}$ :

$$\mathcal{E}_{\text{Noise}} = \mathbb{E}_{\mathbf{x}, \mathbf{X}, \boldsymbol{\Theta}} \left[ \mathbb{E}_{\boldsymbol{\epsilon}} \left[ \hat{f}(\mathbf{x})^2 \right] - \left( \mathbb{E}_{\boldsymbol{\epsilon}} \left[ \hat{f}(\mathbf{x}) \right] \right)^2 \right]. \quad (7)$$

**Initialization variance:** The second term encodes the fluctuations stemming from the random initialization of the random feature vectors,  $\boldsymbol{\Theta}$ :

$$\mathcal{E}_{\text{Init}} = \mathbb{E}_{\mathbf{x}, \mathbf{X}} \left[ \mathbb{E}_{\boldsymbol{\Theta}} \left[ \mathbb{E}_{\boldsymbol{\epsilon}} \left[ \hat{f}(\mathbf{x})^2 \right] \right] - \mathbb{E}_{\boldsymbol{\Theta}, \boldsymbol{\epsilon}} \left[ \hat{f}(\mathbf{x})^2 \right] \right]. \quad (8)$$

**Sampling variance:** The third term measures the fluctuations due to the sampling of the training data,  $\mathbf{X}$ :

$$\mathcal{E}_{\text{Samp}} = \mathbb{E}_{\mathbf{x}} \left[ \mathbb{E}_{\mathbf{X}} \left[ \mathbb{E}_{\boldsymbol{\Theta}, \boldsymbol{\epsilon}} \left[ \hat{f}(\mathbf{x})^2 \right] \right] - \mathbb{E}_{\mathbf{X}, \boldsymbol{\Theta}, \boldsymbol{\epsilon}} \left[ \hat{f}(\mathbf{x})^2 \right] \right]. \quad (9)$$

**Bias:** Finally, the fourth term is the bias, i.e. the error that remains once all the sources of variance have been averaged out. It can be understood as the approximation error of our model and takes the form:

$$\mathcal{E}_{\text{Bias}} = \mathbb{E}_{\mathbf{x}} \left[ \left( \langle \boldsymbol{\beta}, \mathbf{x} \rangle - \mathbb{E}_{\mathbf{X}, \boldsymbol{\Theta}, \boldsymbol{\epsilon}} \left[ \hat{f}(\mathbf{x}) \right] \right)^2 \right]. \quad (10)$$

Note that since we are performing deterministic ridge regression, the noise induced by SGD, which can play an important role outside the lazy regime for deep neural networks, cannot be captured.

**Main result** Consider the high-dimensional limit where the input dimension  $D$ , the hidden layer dimension  $P$  (which is equal to the number of parameter in our model) and the number of training points  $N$  go to infinity with their ratios fixed:

$$N, P, D \rightarrow \infty, \quad \frac{P}{D} = \mathcal{O}(1), \quad \frac{N}{D} = \mathcal{O}(1). \quad (11)$$

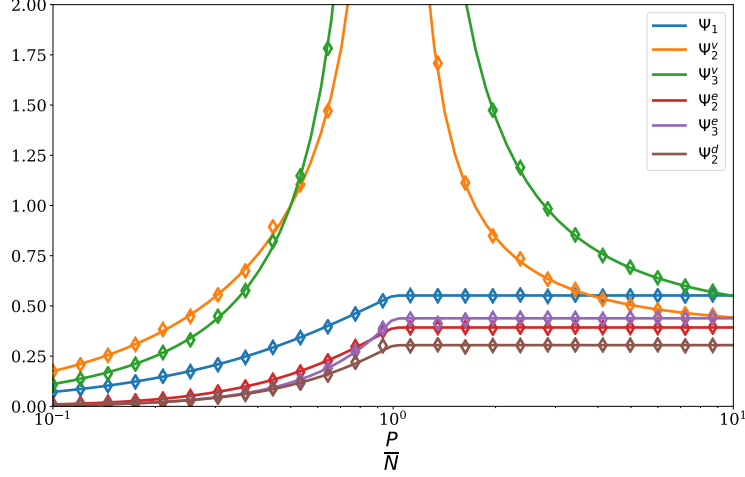


Figure 2: All the terms entering our analytical expressions for the decomposition of the error (Equations 12-17), as function of the overparametrization ratio  $P/N$  for  $\lambda = 10^{-5}$  and  $N/D = 1$ . Numerical estimations obtained for a finite size  $D = 200$  (diamonds) shows that the asymptotic predictions are extremely accurate even at moderate sizes.

We obtain the following result:

$$\mathbb{E}_{\mathbf{x}, \boldsymbol{\varepsilon}, \boldsymbol{\Theta}, \mathbf{X}} [\langle \boldsymbol{\beta}, \mathbf{x} \rangle \hat{f}(\mathbf{x})] = F^2 \Psi_1, \quad (12)$$

$$\mathbb{E}_{\mathbf{x}, \boldsymbol{\Theta}, \mathbf{X}} \left[ \mathbb{E}_{\boldsymbol{\varepsilon}} [\hat{f}(\mathbf{x})]^2 \right] = F^2 \Psi_2^v, \quad (13)$$

$$\mathbb{E}_{\mathbf{x}, \boldsymbol{\Theta}, \mathbf{X}} \left[ \mathbb{E}_{\boldsymbol{\varepsilon}} [\hat{f}(\mathbf{x})^2] - \mathbb{E}_{\boldsymbol{\varepsilon}} [\hat{f}(\mathbf{x})]^2 \right] = \tau^2 \Psi_3^v, \quad (14)$$

$$\mathbb{E}_{\mathbf{x}, \mathbf{X}} \left[ \mathbb{E}_{\boldsymbol{\varepsilon}, \boldsymbol{\Theta}} [\hat{f}(\mathbf{x})]^2 \right] = F^2 \Psi_2^e, \quad (15)$$

$$\mathbb{E}_{\mathbf{x}, \mathbf{X}} \left[ \mathbb{E}_{\boldsymbol{\varepsilon}, \boldsymbol{\Theta}} [\hat{f}(\mathbf{x})^2] - \mathbb{E}_{\boldsymbol{\varepsilon}, \boldsymbol{\Theta}} [\hat{f}(\mathbf{x})]^2 \right] = \tau^2 \Psi_3^e, \quad (16)$$

$$\mathbb{E}_{\mathbf{x}} \left[ \mathbb{E}_{\boldsymbol{\varepsilon}, \boldsymbol{\Theta}, \mathbf{X}} [\hat{f}(\mathbf{x})]^2 \right] = F^2 \Psi_2^d, \quad (17)$$

where the terms  $\{\Psi_1, \Psi_2^v, \Psi_3^v, \Psi_2^e, \Psi_3^e, \Psi_2^d\}$ , whose full analytical expressions are deferred to Appendix B, are computed following the steps below:

1. *Mapping to a random matrix theory problem.* The first step is to express the right-hand sides of Equations 12-17 as traces over random matrices. This is achieved by replacing our model with its asymptotically equivalent Gaussian covariate model [11], in which the non-linearity of the activation function is encoded as an extra noise term. This enables to take the expectation value with respect to the test sample  $\mathbf{x}$ .
2. *Mapping to a statistical physics model.* The random matrix theory problem resulting from the solution of ridge regression (4) involves inverse random matrices. In order to evaluate their expectation value, we use the formula:

$$M_{ij}^{-1} = \lim_{n \rightarrow 0} \int \prod_{\alpha=1}^n \prod_{i=1}^D d\eta_i^\alpha \eta_i^1 \eta_j^1 e^{-\frac{1}{2} \eta_i^\alpha M_{ij} \eta_j^\alpha},$$

which is based on the Replica Trick [34, 49]. The Gaussian integrals over  $\boldsymbol{\varepsilon}, \boldsymbol{\Theta}, \mathbf{X}$  can then be straightforwardly performed and lead to a Statistical Physics model for the auxiliary variables  $\eta_i^\alpha$ .

3. *Mean-Field Theory.* The model for the  $\eta_i^\alpha$  variables can then be solved by introducing as order parameters the  $n \times n$  overlap matrices  $Q^{\alpha\beta} = \frac{1}{P} \sum_{i=1}^P \eta_i^\alpha \eta_i^\beta$  and using replica theory [34], see Appendix C for the detailed computation<sup>3</sup>.

<sup>3</sup>In order to obtain the asymptotic formulas for the  $\Psi$ 's we need to compute (what are called in the Statistical Physics jargon) fluctuations around mean-field theory.

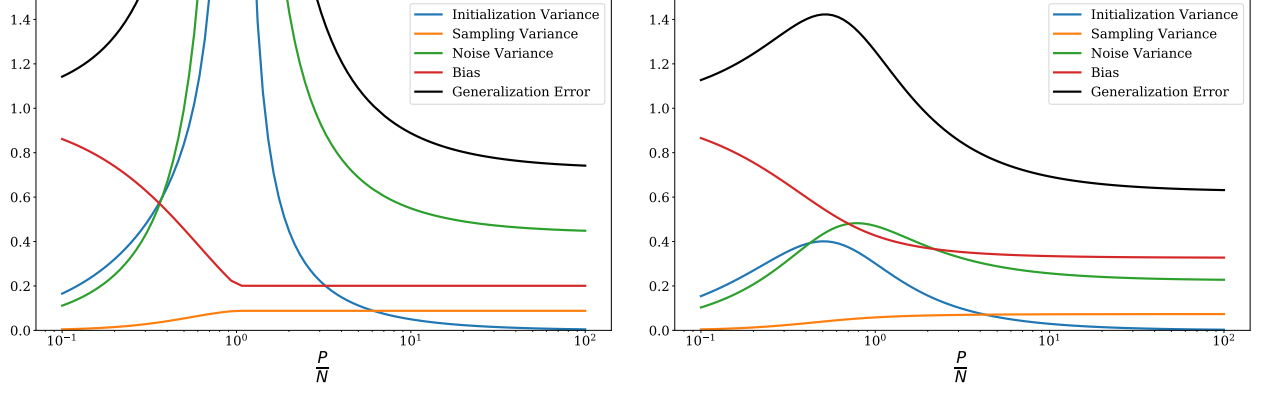


Figure 3: Decomposition of the test error into the bias and the various sources of variance as function of the overparametrization ratio  $P/N$  for  $N/D = 1$ ,  $\text{SNR} = F/\tau = 1$ . Two values of the regularization constant are used:  $\lambda = 10^{-5}$  (left) and  $\lambda = 10^{-1}$  (right). Notice the contrasting behaviors at the interpolation threshold: the noise and initialization variances diverge then decrease monotonically whereas the sampling variance and the bias display a kink followed by a plateau. These singular behaviors are smoothed out by regularization.

The  $\Psi$ 's may also be estimated numerically at finite size by evaluating the traces of the random matrices appearing in the Gaussian covariate model at the end of step 1. Figure 2 shows that results thus obtained are in excellent agreement with the asymptotic expressions even at moderate sizes, e.g.  $D = 200$ , proving the robustness of steps 2 and 3, which differ from the approach presented in [11].

The indices  $v, e, d$  in  $\{\Psi_1, \Psi_2^v, \Psi_3^v, \Psi_2^e, \Psi_3^e, \Psi_2^d\}$  stand for *vanilla*, *ensemble* and *divide and conquer*. The *vanilla* terms are sufficient to obtain the test error of a single RF model and were computed in [11]. The *ensemble* and *divide and conquer* terms allow to obtain the test error obtained when averaging the predictions of several different learners trained respectively on the same dataset and on different splits of the original dataset (see section 5). Figure 2 shows that the *vanilla* terms exhibit a radically different behavior from the others: at vanishing regularization, they diverge at  $P = N$  then decrease monotonically, whereas the others display a kink followed by a plateau. This behavior will be key to the following analysis.

## 4 Analysis of Bias and Variances

The results of the previous section, allow to rewrite the decomposition of the test error as follows:

$$\mathcal{E}_{\text{Noise}} = \tau^2 \Psi_3^v, \quad (18)$$

$$\mathcal{E}_{\text{Init}} = F^2 (\Psi_2^v - \Psi_2^e), \quad (19)$$

$$\mathcal{E}_{\text{Samp}} = F^2 (\Psi_2^e - \Psi_2^d), \quad (20)$$

$$\mathcal{E}_{\text{Bias}} = F^2 (1 - 2\Psi_1 + \Psi_2^d). \quad (21)$$

These contributions, together with the test error, are shown in figure 3 in the case of small (top) and large (bottom) regularization.

**Interpolation Threshold** The peak at the interpolation threshold is completely due to noise and initialization variance, which both diverge at vanishing regularization. In contrast, the sampling variance and the bias remain finite and exhibit a phase transition at  $P = N$ , which is revealed by a kink at vanishing regularization. Adding regularization smooths out these singular behaviours: it removes the divergence and irons out the kink.

**Overparametrized regime** In the overparametrized regime, the sampling variance and the bias do not vary substantially (they remain constant for vanishing regularization). The decrease of the test error is entirely due to the decrease of the noise and initialization variances for  $P > N$ . In the limit  $P/N \rightarrow \infty$ , the initialization variance vanishes, whereas there remains an irreducible noise variance.

**Discussion** In conclusion, we find that the *origin of the double descent curve lies in the behavior of noise and initialization variances*. The benefit of overparametrizing stems only from reducing these two contributions.

These results are qualitatively similar to the empirical decomposition of [9] for real neural networks. The divergence of the test error as  $(P/N - 1)^{-1}$  at the interpolation threshold is in agreement with the results of [11]<sup>4</sup>. As for the decrease of the test error in the over-parametrized regime, we find consistently with the scaling arguments of [1] that the initialization error asymptotically decays to zero inversely proportional to the width (see Appendix A.1 for more details). The interpretation of our results differ from those of [11] where the authors relate the over-fitting peak occurring at  $P = N$  to a divergence in both the variance and the bias terms. This is due to the fact the bias term, as defined in that paper, also includes the initialization variance<sup>5</sup>. When the two are disentangled, it becomes clear that it is only the latter which is responsible for the divergence: the bias is, in fact, well-behaved at  $P = N$ .

**Intuition** The phenomenology described above can be understood by noting that the model essentially performs linear regression, learning a vector  $\mathbf{a} \in \mathbb{R}^P$  on a projected dataset  $\mathbf{Z} \in \mathbb{R}^{N \times P}$  (the activations of the hidden nodes of the RF network). Since  $\mathbf{a}$  is constrained to lie in the space spanned by  $\mathbf{Z}$ , which is of dimension  $\min(N, P)$ , the model gains expressivity when  $P$  increases while staying smaller than  $N$ .

At  $P = N$ , the problem becomes fully determined: the data is perfectly interpolated for vanishing  $\lambda$ . Two types of noise are overfit: (i) the *stochastic noise* corrupting the labels, yielding the divergence in noise variance, and (ii) the *deterministic noise* stemming from the non-linearity of the activation function which cannot be captured, yielding the divergence in initialization variance. However, by further increasing  $P$ , the noise is spread over more and more random features and is effectively averaged out. Consequently, the test error decreases again as  $P$  increases.

When we make the problem deterministic by averaging out all sources of randomness, i.e. by considering the bias, we see that increasing  $P$  beyond  $N$  has no effect whatsoever. Indeed, the extra degrees of freedom, which lie in the null space of  $\mathbf{Z}$ , do not provide any extra expressivity: at vanishing regularization, they are killed by the pseudo-inverse to reach the minimum norm solution. For non-vanishing  $\lambda$ , a similar phenomenology is observed but the interpolation threshold is reached slightly after  $P = N$  since the expressivity of the learner is lowered by regularization.

## 5 On the effect of ensembling

In order to further study the effect of the variances on the test error, we follow [1] and study the impact of ensembling. In the lazy regime of deep neural networks, the initial values of the weights only affect the gradient at initialization, which corresponds to the vector of random features. Hence, we can study the effect of ensembling in the lazy regime by averaging the predictions of RF models with independently drawn random feature vectors.

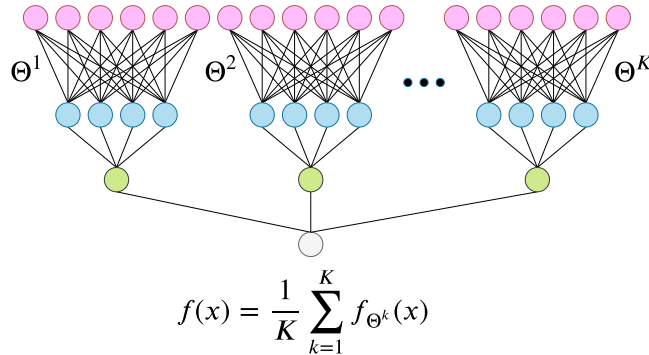


Figure 4: Illustration of the ensembling procedure over  $K$  Random Features networks trained on the same data but with different realizations of the first layer,  $\{\Theta_1, \dots, \Theta_K\}$ .

**Expression of the test error** Consider a set of  $K > 1$  RF networks whose first layer weights are drawn independently. These networks are trained independently on the *same* training set. In the analogy outlined above, they correspond to  $K$  independent initializations of the neural network. At the end of training, one obtains  $K$  estimators  $\{\hat{f}_{\Theta^k}\}$  ( $k = 1, \dots, K$ ). When a new sample  $\mathbf{x}$  is presented to the system, the output is

<sup>4</sup>Note that for classification problems the singularity is different [1].

<sup>5</sup>For a given set of random features this is legitimate, but from the perspective of lazy learning the randomness in the features corresponds to the one due to initialization, which is an additional source of variance.



taken to be the average over the outputs of the  $K$  networks, as illustrated in figure 4. By expanding the square and taking the expectation with respect to the random initializations, the test error can then be written as:

$$\begin{aligned}\mathbb{E}_{\{\Theta^k\}}[\mathcal{R}_{\text{RF}}] &= \mathbb{E}_{\mathbf{x}} \left[ \left( \langle \beta, \mathbf{x} \rangle - \frac{1}{K} \sum_k \hat{f}_{\Theta^k}(\mathbf{x}) \right)^2 \right] \\ &= \mathbb{E}_{\mathbf{x}} [\langle \beta, \mathbf{x} \rangle^2] - \frac{2}{K} \sum_{i=1}^K \mathbb{E}_{\mathbf{x}} [\langle \beta, \mathbf{x} \rangle \hat{f}_{\Theta^i}(\mathbf{x})] + \frac{1}{K^2} \sum_{i,j=1}^K \mathbb{E}_{\mathbf{x}} [\hat{f}_{\Theta^i}(\mathbf{x}) \hat{f}_{\Theta^j}(\mathbf{x})].\end{aligned}\quad (22)$$

The key here is to isolate in the double sum the  $K(K-1)$  *ensemble* terms  $i \neq j$ , which involve two different initializations and yield  $\mathbb{E}_{\mathbf{x}} [\mathbb{E}_{\Theta} [\hat{f}_{\Theta}(\mathbf{x})]^2]$ , from the  $K$  *vanilla* terms which give  $\mathbb{E}_{\mathbf{x}, \Theta} [\hat{f}_{\Theta}(\mathbf{x})^2]$ . This allows to express the test error in terms of the quantities defined in (12) to (17) and leads to the analytic formula for the test error valid for any  $K \in \mathbb{N}$ :

$$\mathbb{E}_{\{\Theta^{(k)}\}, \mathbf{X}, \epsilon}[\mathcal{R}_{\text{RF}}] = F^2 (1 - 2\Psi_1^v) + \frac{1}{K} (F^2 \Psi_2^v + \tau^2 \Psi_3^v) + \left(1 - \frac{1}{K}\right) (F^2 \Psi_2^e + \tau^2 \Psi_3^e). \quad (23)$$

We see that ensembling amounts to a linear interpolation between the *vanilla* terms  $\Psi_2^v, \Psi_3^v$ , for  $K = 1$ , and the *ensemble* terms  $\Psi_2^e, \Psi_3^e$  for  $K \rightarrow \infty$ .

The effect of ensembling on the double descent curve is shown in figure 5. As  $K$  increases, the overfitting peak at the interpolation threshold is diminished. This observation is very similar to the empirical findings of [1] in the context of real neural networks. Our analytic expression agrees with the numerical results obtained by training RF models, even at moderate size  $D = 200$ .

Note that a related procedure is the *divide and conquer* approach, where the dataset is partitioned into  $K$  splits of equal size and each one of the  $K$  differently initialized learners is trained on a distinct split. This approach was studied for kernel learning in [46], and is analyzed within our framework in Appendix A.2.

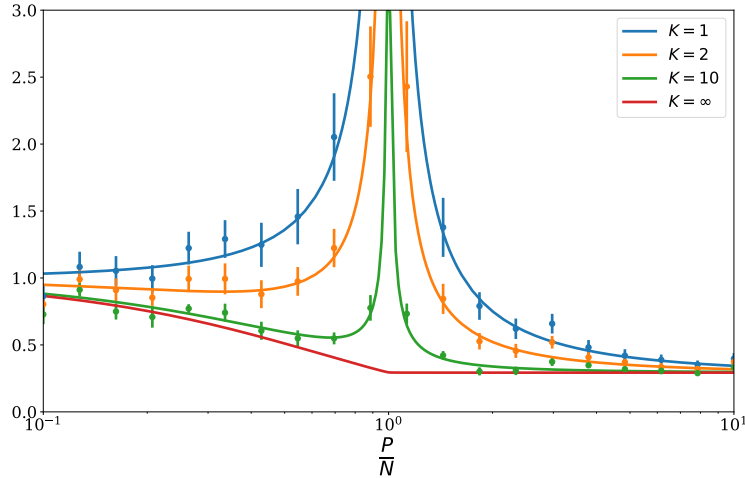


Figure 5: Test error when ensembling  $K = 1, 2, 10$  differently initialized RF models as function of the over-parametrization ratio  $P/N$ . We fixed  $\lambda = 10^{-5}$ ,  $N/D = 1$ ,  $\text{SNR} = 10$ . For comparison, we show the results of numerical simulations at finite  $D = 200$ : the vertical bars depict the standard deviation over 10 runs. The variability observed here was absent in figure 2 because we are considering the true RF model rather than the asymptotically equivalent Gaussian covariate model. This shows that most of this variability is caused by the finite-size deviation between the two models. Note that our analytic expression (23) gives us access to the limit  $N \rightarrow \infty$ , where the divergence at  $P = N$  is entirely suppressed.



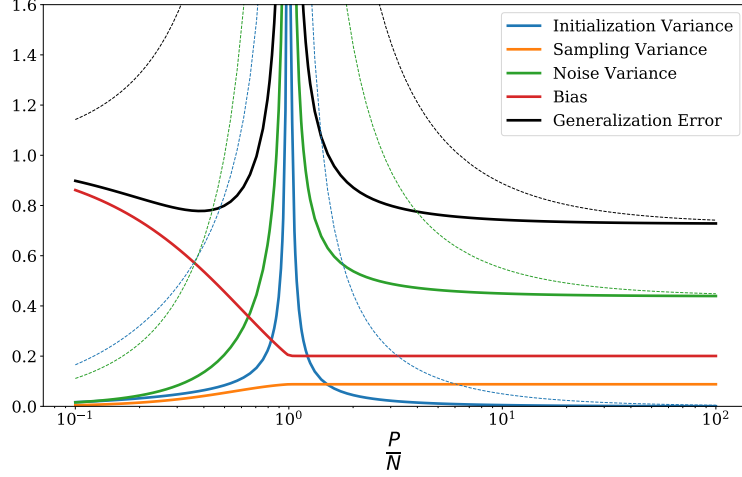


Figure 6: Decomposition of the test error into the bias and the various sources of variance as function of the overparametrization ratio  $P/N$  for  $\lambda = 10^{-5}$ ,  $N/D = 1$ ,  $\text{SNR} = 1$ . The thin dashed lines are taken from figure 3 (top) where we had  $K = 1$ ; the thick solid lines show how ensembling at  $K = 10$  suppressed the divergences of the noise and initialization variances.

**Ensembling reduces the double trouble** The bias-variance decomposition of the test error makes the suppression of the divergence explicit. The bias and variances contribution read for the averaged estimator:

$$\mathcal{E}_{\text{Noise}} = \tau^2 \left( \Psi_3^e + \frac{1}{K} (\Psi_3^v - \Psi_3^e) \right), \quad (24)$$

$$\mathcal{E}_{\text{Init}} = \frac{F^2}{K} (\Psi_2^v - \Psi_2^e), \quad (25)$$

$$\mathcal{E}_{\text{Samp}} = F^2 (\Psi_2^e - \Psi_2^d), \quad (26)$$

$$\mathcal{E}_{\text{Bias}} = F^2 (1 - 2\Psi_1 + \Psi_2^d). \quad (27)$$

These equations show that ensembling only affects the noise and initialization variances. In both cases, their divergence at the interpolation threshold (due to  $\Psi_2^v, \Psi_3^v$ ) is suppressed as  $1/K$ , see figure 6 for an illustration. At  $P > N$ , ensembling and overparametrizing have a very similar effect: they wipe out these two troubling sources of randomness by averaging them out over more random features. In fact, we see in figure 5 that a single infinitely overparametrized system ( $K=1$ ,  $P/N \rightarrow \infty$ ) is equivalent to an infinitely ensembled overparametrized system ( $K \rightarrow \infty$ ,  $P > N$ ): in both cases, the system converges to the same kernel limit.

**Ensembling vs. overparametrization** As we have shown, ensembling and overparametrizing have similar effects in the lazy regime. But which is more powerful: ensembling  $K$  models, or using a single model with  $K$  times more features? The answer is given in figure 7 for  $K = 2$  where we plot our analytical results while varying the number of data points,  $N$ . Two observations are particularly interesting. First, overparametrization shifts the interpolation threshold, opening up a region where ensembling outperforms overparametrizing. Second, overparametrization yields a higher asymptotic improvement in the large dataset limit  $N/D \rightarrow \infty$ , but the gap between overparametrizing and ensembling is reduced as  $P/D$  increases. At  $P \gg D$ , where we are already close to the kernel limit, both methods yield a similar improvement. Note that from the point of view of efficiency, ridge regression involves the inversion of a  $P \times P$  matrix, therefore ensembling is significantly more efficient.

**Ensembling vs. optimal regularization** In all the results presented above, we keep the regularization constant  $\lambda$  fixed. However, by appropriately choosing the value of  $\lambda$  at each value of  $P/N$ , the performance is improved. As figure 7 (left) reveals, the optimal value of  $\lambda$  decreases with  $K$  since the minimum of the test error shifts to the left when increasing  $K$ . In other words, ensembling is best when the predictors one ensembles upon are individually under-regularized, as was observed previously for kernel learning in [50]. Figure 8 (right) shows that an infinitely ensembled model ( $K \rightarrow \infty$ ) always performs better than an optimally regularized single model ( $K = 1$ ).

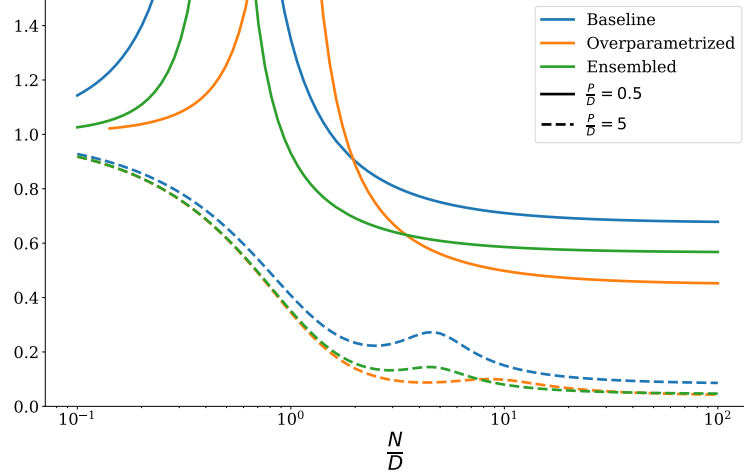


Figure 7: Comparison of the test error of a RF model (blue) with that obtained by doubling the number features (orange) or ensembling over two initializations of the features (green), as function of  $N/D$ . The parameters are  $\lambda = 10^{-5}$ ,  $\text{SNR} = 10$ ,  $P/D = 0.5$  (solid lines) and  $P/D = 5$  (dashed lines).

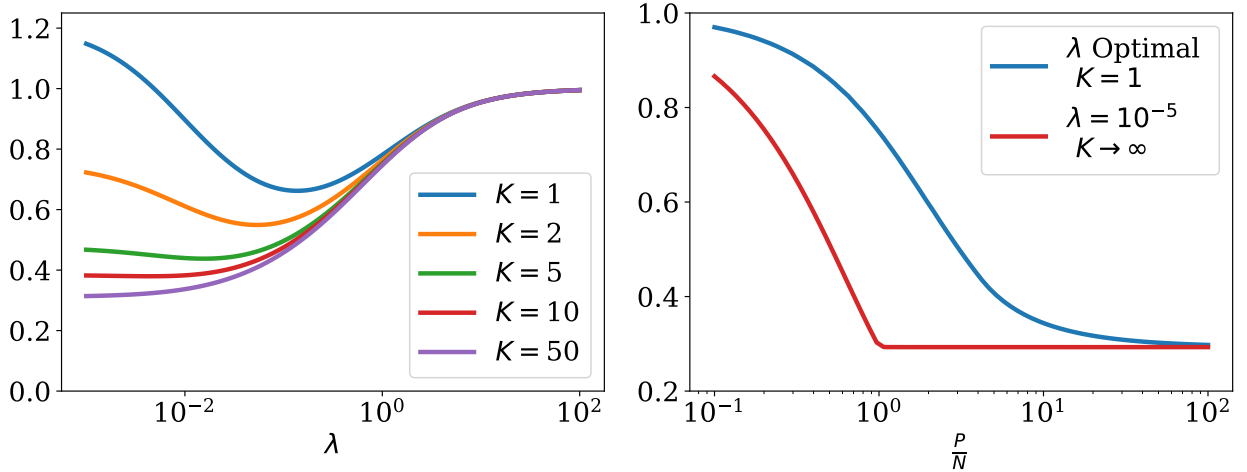


Figure 8: **Left:** Test error as a function of  $\lambda$  for various values of  $K$  and parameters  $P/D = 2$ ,  $N/D = 1$ ,  $\text{SNR} = 10$ . **Right:** Comparison of test error for an optimal regularized system with  $K = 1$  and the system with  $K \rightarrow \infty$  with  $\lambda = 10^{-5}$ . Optimization performed over 50 values of  $\lambda$  from  $10^{-5}$  to  $10^2$ . Parameters are  $N/D = 1$ ,  $\text{SNR} = 10$ .

## 6 Numerical experiments on neural networks

Finally, we investigate whether the phenomenology described here holds for realistic neural networks learning real data in the lazy regime. We follow here the protocol used in [1, 27] and train a 5-layer fully-connected network on the CIFAR-10 dataset. We keep only the first ten PCA components of the images, and divide the images in two classes according to the parity of the labels. We perform  $10^5$  steps of full-batch gradient descent with the *Adam* optimizer and a learning rate of 0.1, and scale the weights as prescribed in [31].

We gradually go from the usual *feature learning* regime to the *lazy learning* regime using the trick introduced in [23], which consists in scaling the output of the network by a factor  $\alpha$  and replacing the learning function  $f_\theta(\mathbf{x})$  by  $\alpha(f_\theta(\mathbf{x}) - f_{\theta_0}(\mathbf{x}))$ . For  $\alpha \gg 1$ , one must have that  $\theta - \theta_0 \sim 1/\alpha$  in order for the learning function to remain of order one. In other words, the weights are forced to stay close to their initialization, hence the name *lazy learning*.

Results are shown in figure 9. Close to the lazy regime ( $\alpha = 100$ , right panel), a very similar behavior as the RF model is observed. The test error curve<sup>6</sup> obtained when ensembling  $K = 20$  independently initialized networks becomes roughly flat after the interpolation threshold (which here is signalled by the peak in the test

<sup>6</sup>Note that we are considering a binary classification task here: the error is defined as the fraction of misclassified images.

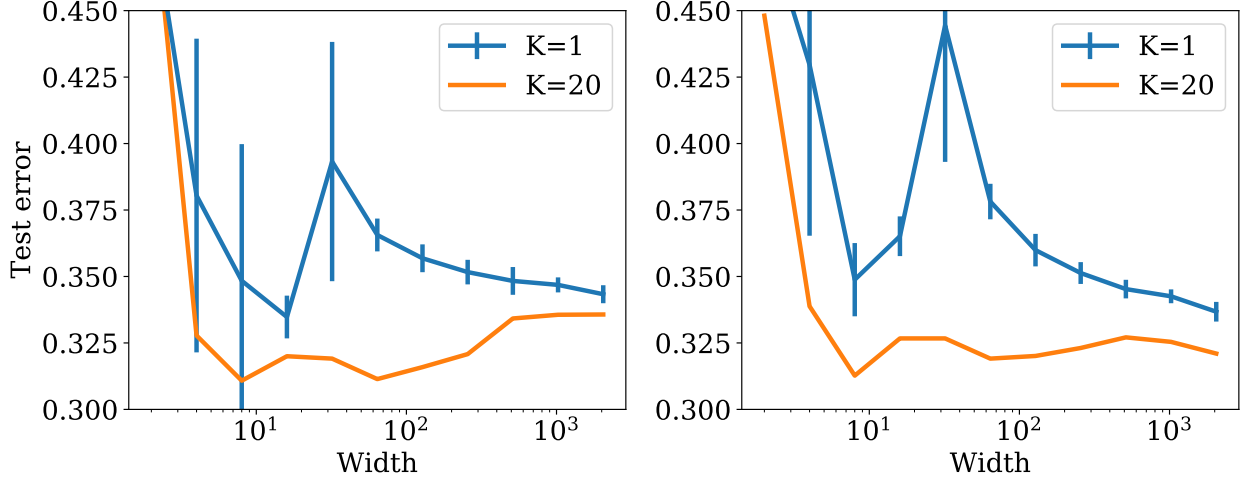


Figure 9: Test error on the binary 10-PCA CIFAR10 as function of the number of nodes per layer of the 5-layer neural network trained until convergence with the full-batch *Adam*. We compare the test error of a single predictor ( $K = 1$ ), averaged over 20 initializations of the weights (the standard deviation is depicted as vertical bars), with the ensembling predictor at  $K = 20$ . **Left:**  $\alpha = 10$ . **Right:**  $\alpha = 100$ , where we are closer to the lazy regime and the ensembling curve flattens beyond the interpolation threshold, which occurs around 30 nodes per layer.

accuracy). As we move away from the lazy regime ( $\alpha=10$ , left panel), the same curve develops a *dip* around the interpolation threshold and increases beyond  $P > N$  as observed previously in [1]. This may arguably be associated to the beneficial effect of *feature learning*, as discussed in [27] where the transition from lazy to feature learning was investigated.

**Acknowledgements** We thank Matthieu Wyart and Lenka Zdeborová for discussions related to this project. This work is supported by the French Agence Nationale de la Recherche under grant ANR-17-CE23-0023-01 PAIL and ANR-19-P3IA-0001 PRAIRIE, and by the Simons Foundation (#454935, Giulio Biroli). We also acknowledge support from the chaire CFM-ENS “Science des données”.

## References

- [1] Mario Geiger, Arthur Jacot, Stefano Spigler, Franck Gabriel, Levent Sagun, Stéphane d’Ascoli, Giulio Biroli, Clément Hongler, and Matthieu Wyart. Scaling description of generalization with number of parameters in deep learning. *arXiv preprint arXiv:1901.01608*, 2019.
- [2] Alex Krizhevsky, Ilya Sutskever, and Geoffrey E Hinton. Imagenet classification with deep convolutional neural networks. In *Advances in neural information processing systems*, pages 1097–1105, 2012.
- [3] Yann LeCun, Yoshua Bengio, and Geoffrey Hinton. Deep learning. *nature*, 521(7553):436–444, 2015.
- [4] Geoffrey Hinton, Li Deng, Dong Yu, George E Dahl, Abdel-rahman Mohamed, Navdeep Jaitly, Andrew Senior, Vincent Vanhoucke, Patrick Nguyen, Tara N Sainath, et al. Deep neural networks for acoustic modeling in speech recognition: The shared views of four research groups. *IEEE Signal processing magazine*, 29(6):82–97, 2012.
- [5] Ilya Sutskever, Oriol Vinyals, and Quoc V Le. Sequence to sequence learning with neural networks. In *Advances in neural information processing systems*, pages 3104–3112, 2014.
- [6] Chiyuan Zhang, Samy Bengio, Moritz Hardt, Benjamin Recht, and Oriol Vinyals. Understanding deep learning requires rethinking generalization. *arXiv preprint arXiv:1611.03530*, 2016.
- [7] Madhu S Advani and Andrew M Saxe. High-dimensional dynamics of generalization error in neural networks. *arXiv preprint arXiv:1710.03667*, 2017.
- [8] Mikhail Belkin, Daniel Hsu, Siyuan Ma, and Soumik Mandal. Reconciling modern machine learning and the bias-variance trade-off. *arXiv preprint arXiv:1812.11118*, 2018.
- [9] Brady Neal, Sarthak Mittal, Aristide Baratin, Vinayak Tantia, Matthew Scicluna, Simon Lacoste-Julien, and Ioannis Mitliagkas. A modern take on the bias-variance tradeoff in neural networks. *arXiv preprint arXiv:1810.08591*, 2018.
- [10] Trevor Hastie, Andrea Montanari, Saharon Rosset, and Ryan J Tibshirani. Surprises in high-dimensional ridgeless least squares interpolation. *arXiv preprint arXiv:1903.08560*, 2019.
- [11] Song Mei and Andrea Montanari. The generalization error of random features regression: Precise asymptotics and double descent curve. *arXiv preprint arXiv:1908.05355*, 2019.
- [12] Behnam Neyshabur, Ryota Tomioka, and Nathan Srebro. In search of the real inductive bias: On the role of implicit regularization in deep learning. *arXiv preprint arXiv:1412.6614*, 2014.
- [13] Stefano Spigler, Mario Geiger, Stéphane d’Ascoli, Levent Sagun, Giulio Biroli, and Matthieu Wyart. A jamming transition from under-to over-parametrization affects loss landscape and generalization. *arXiv preprint arXiv:1810.09665*, 2018.
- [14] Preetum Nakkiran, Gal Kaplun, Yamini Bansal, Tristan Yang, Boaz Barak, and Ilya Sutskever. Deep double descent: Where bigger models and more data hurt. *arXiv preprint arXiv:1912.02292*, 2019.
- [15] Leo Breiman. Reflections after refereeing papers for nips. *The Mathematics of Generalization*, pages 11–15, 1995.
- [16] Manfred Opper and Wolfgang Kinzel. Statistical mechanics of generalization. In *Models of neural networks III*, pages 151–209. Springer, 1996.
- [17] Andrea J Liu and Sidney R Nagel. Jamming is not just cool any more. *Nature*, 396(6706):21–22, 1998.
- [18] Andreas Engel and Christian Van den Broeck. *Statistical mechanics of learning*. Cambridge University Press, 2001.
- [19] Silvio Franz and Giorgio Parisi. The simplest model of jamming. *Journal of Physics A: Mathematical and Theoretical*, 49(14):145001, 2016.
- [20] Florent Krzakala and Jorge Kurchan. Landscape analysis of constraint satisfaction problems. *Physical Review E*, 76(2):021122, 2007.

- [21] Lenka Zdeborová and Florent Krzakala. Phase transitions in the coloring of random graphs. *Physical Review E*, 76(3):031131, 2007.
- [22] Saharon Rosset, Ji Zhu, and Trevor J Hastie. Margin maximizing loss functions. In *Advances in neural information processing systems*, pages 1237–1244, 2004.
- [23] Lénaïc Chizat, Edouard Oyallon, and Francis Bach. On lazy training in differentiable programming. In H. Wallach, H. Larochelle, A. Beygelzimer, F. d’Alché Buc, E. Fox, and R. Garnett, editors, *Advances in Neural Information Processing Systems 32*, pages 2933–2943. Curran Associates, Inc., 2019.
- [24] Sanjeev Arora, Simon S Du, Wei Hu, Zhiyuan Li, Ruslan Salakhutdinov, and Ruosong Wang. On exact computation with an infinitely wide neural net. *arXiv preprint arXiv:1904.11955*, 2019.
- [25] Song Mei, Theodor Misiakiewicz, and Andrea Montanari. Mean-field theory of two-layers neural networks: dimension-free bounds and kernel limit. *arXiv preprint arXiv:1902.06015*, 2019.
- [26] Blake Woodworth, Suriya Gunasekar, Jason Lee, Daniel Soudry, and Nathan Srebro. Kernel and deep regimes in overparametrized models. *arXiv preprint arXiv:1906.05827*, 2019.
- [27] Mario Geiger, Stefano Spigler, Arthur Jacot, and Matthieu Wyart. Disentangling feature and lazy learning in deep neural networks: an empirical study. *arXiv preprint arXiv:1906.08034*, 2019.
- [28] Sanjeev Arora, Simon S Du, Zhiyuan Li, Ruslan Salakhutdinov, Ruosong Wang, and Dingli Yu. Harnessing the power of infinitely wide deep nets on small-data tasks. *arXiv preprint arXiv:1910.01663*, 2019.
- [29] Amit Daniely, Roy Frostig, and Yoram Singer. Toward deeper understanding of neural networks: The power of initialization and a dual view on expressivity. In *Advances In Neural Information Processing Systems*, pages 2253–2261, 2016.
- [30] Jaehoon Lee, Yasaman Bahri, Roman Novak, Samuel S Schoenholz, Jeffrey Pennington, and Jascha Sohl-Dickstein. Deep neural networks as gaussian processes. *arXiv preprint arXiv:1711.00165*, 2017.
- [31] Arthur Jacot, Franck Gabriel, and Clément Hongler. Neural tangent kernel: Convergence and generalization in neural networks. In *Advances in neural information processing systems*, pages 8571–8580, 2018.
- [32] Ali Rahimi and Benjamin Recht. Random features for large-scale kernel machines. In *Advances in neural information processing systems*, pages 1177–1184, 2008.
- [33] Behnam Neyshabur, Ryota Tomioka, Ruslan Salakhutdinov, and Nathan Srebro. Geometry of optimization and implicit regularization in deep learning. *arXiv preprint arXiv:1705.03071*, 2017.
- [34] Marc Mézard, Giorgio Parisi, and Miguel Virasoro. *Spin glass theory and beyond: An Introduction to the Replica Method and Its Applications*, volume 9. World Scientific Publishing Company, 1987.
- [35] Hyunjun Sebastian Seung, Haim Sompolinsky, and Naftali Tishby. Statistical mechanics of learning from examples. *Physical review A*, 45(8):6056, 1992.
- [36] Madhu Advani, Subhaneil Lahiri, and Surya Ganguli. Statistical mechanics of complex neural systems and high dimensional data. *Journal of Statistical Mechanics: Theory and Experiment*, 2013(03):P03014, 2013.
- [37] Lenka Zdeborová and Florent Krzakala. Statistical physics of inference: Thresholds and algorithms. *Advances in Physics*, 65(5):453–552, 2016.
- [38] Giacomo Livan, Marcel Novaes, and Pierpaolo Vivo. *Introduction to random matrices: theory and practice*, volume 26. Springer, 2018.
- [39] Elena Tarquini, Giulio Biroli, and Marco Tarzia. Level statistics and localization transitions of levy matrices. *Physical review letters*, 116(1):010601, 2016.
- [40] Amol Aggarwal, Patrick Lopatto, and Horng-Tzer Yau. Goe statistics for levy matrices. *arXiv preprint arXiv:1806.07363*, 2018.
- [41] Preetum Nakkiran. More data can hurt for linear regression: Sample-wise double descent. *arXiv preprint arXiv:1912.07242*, 2019.

- [42] Mikhail Belkin, Daniel Hsu, and Ji Xu. Two models of double descent for weak features. *arXiv preprint arXiv:1903.07571*, 2019.
- [43] Zeyu Deng, Abba Kammoun, and Christos Thrampoulidis. A model of double descent for high-dimensional binary linear classification. *arXiv preprint arXiv:1911.05822*, 2019.
- [44] Ganesh Kini and Christos Thrampoulidis. Analytic study of double descent in binary classification: The impact of loss. *arXiv preprint arXiv:2001.11572*, 2020.
- [45] Florent Krzakala Marc Mézard Lenka Zdeborová Federica Gerace, Bruno Loureiro. Generalisation error in learning with random features and the hidden manifold model. *arXiv:2002.09339*, 2020.
- [46] Harris Drucker, Corinna Cortes, Lawrence D Jackel, Yann LeCun, and Vladimir Vapnik. Boosting and other ensemble methods. *Neural Computation*, 6(6):1289–1301, 1994.
- [47] Yuchen Zhang, John Duchi, and Martin Wainwright. Divide and conquer kernel ridge regression. In *Conference on Learning Theory*, pages 592–617, 2013.
- [48] Sebastian Goldt, Marc Mézard, Florent Krzakala, and Lenka Zdeborová. Modelling the influence of data structure on learning in neural networks. *arXiv preprint arXiv:1909.11500*, 2019.
- [49] Joël Bun, Jean-Philippe Bouchaud, and Marc Potters. Cleaning correlation matrices. *Risk magazine*, 2015, 2016.
- [50] Yuchen Zhang, John Duchi, and Martin Wainwright. Divide and conquer kernel ridge regression: A distributed algorithm with minimax optimal rates. *The Journal of Machine Learning Research*, 16(1):3299–3340, 2015.
- [51] Nitesh V Chawla, Thomas E Moore, Lawrence O Hall, Kevin W Bowyer, W Philip Kegelmeyer, and Clayton Springer. Distributed learning with bagging-like performance. *Pattern recognition letters*, 24(1-3):455–471, 2003.

## A Further analytical results

### A.1 Asymptotic scalings

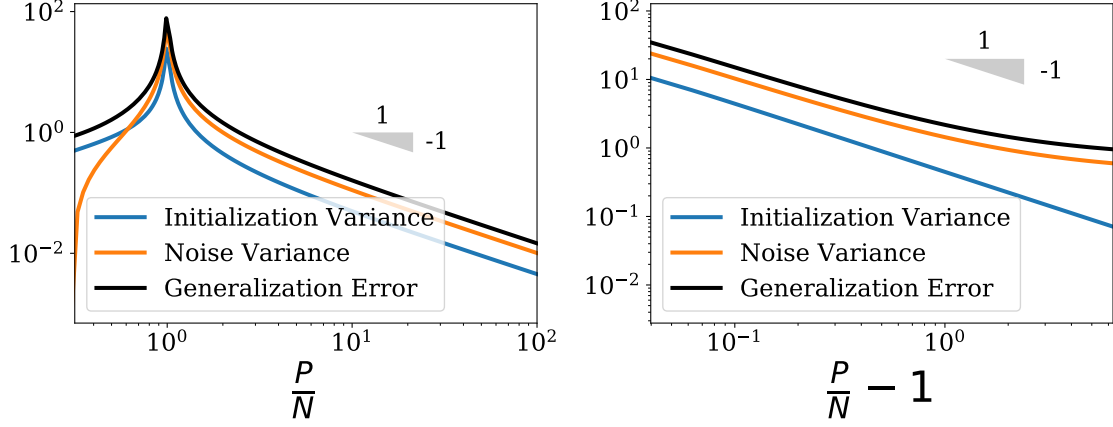


Figure 10: Log-log behaviour of the quantities of interest at **Left**:  $P/N \rightarrow \infty$  and **Right**:  $P \rightarrow N$  with  $\lambda = 10^{-5}$ ,  $N/D = 1$  and  $\tau = 1$ . In both cases, one observes an inverse scaling law.

Figure 10 (left) shows that the various terms entering the decomposition of the generalization error approach their asymptotic values at a rate  $(P/N)^{-1}$ . This scaling law is consistent with that found in [1] for real neural networks, where  $P$  is replaced by the width of the layers of the network. As for the divergence of the noise and initialization variances observed at the interpolation threshold, figure 10 (right) shows that they also follow an inverse power law  $(P/N - 1)^{-1}$  at vanishing regularization.

### A.2 Divide and Conquer approach

As mentioned in the main text, another way to average the predictions of differently initialized learners is the *divide and conquer* approach [46]. In this framework, the data set is divided into  $K$  splits of size  $N/K$ . Each of the  $K$  differently initialized learner is trained on a distinct split. This approach is extremely useful for kernel learning [50], where the computational burden is in the inversion of the Gram matrix which is of size  $N \times N$ . In the random projection approach considered here, it does not offer any computational gain, however it is interesting how it affects the generalization error.

Within our framework, the generalization error can easily be calculated as:

$$\mathbb{E}_{\{\Theta^{(k)}\}, \mathbf{X}, \epsilon} [\mathcal{R}_{\text{RF}}] = F^2 (1 - 2\Psi_1^v) + \frac{1}{K} (F^2 \Psi_2^v + \tau^2 \Psi_3^v) + \left(1 - \frac{1}{K}\right) F^2 \Psi_2^d, \quad (28)$$

where the effective number of data points which enters this formula is  $N_{\text{eff}} = N/K$  due to the splitting of the training set.

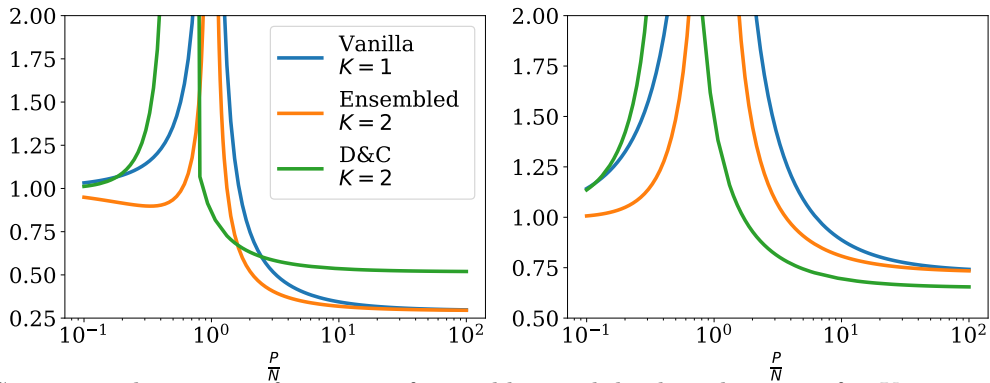


Figure 11: Comparison between performances of ensembling and divide and conquer for  $K = 2$  at different SNR. **Left**:  $\text{SNR} = F/\tau = 10$ . **Right**:  $\text{SNR} = F/\tau = 1$ . Computations performed with fixed  $N/D = 1$ ,  $F = 1$  and  $\lambda = 10^{-5}$ .



Comparing the previous expression with that obtained for ensembling (49) is instructive: here, increasing  $K$  replaces the *vanilla* terms  $\Psi_2^v, \Psi_3^v$  by the *divide and conquer* term  $\Psi_2^d$ . This shows that divide and conquer has a *denoising* effect: at  $K \rightarrow \infty$ , the effect of the additive noise on the labels is completely suppressed. This was not the case for ensembling. The price to pay is that  $N_{\text{eff}}$  decreases, hence one is shifted to the underparametrized regime.

In Figure 11, we see that the kernel limit error of the divide and conquer approach, i.e. the asymptotic value of the error at  $P/N \rightarrow \infty$ , is different from the usual kernel limit error, since the effective dataset is two times smaller at  $K = 2$ . The denoising effect of the divide and conquer approach is illustrated by the fact that its kernel limit error is higher at high SNR, but lower at low SNR. This is of practical relevance, and is much related to the beneficial effect of *bagging* in noisy dataset scenarios. The divide and conquer approach, which only differs from bagging by the fact that the different partitions of the dataset are disjoint, was shown to reach bagging-like performance in various setups such as decision trees and neural networks [51].

### A.3 Is it always better to be overparametrized ?

A common thought is that the double descent curve always reaches its minimum in the over-parametrized regime, leading to the idea that the corresponding model "cannot overfit". In this section, we show that this is not always the case. Three factors tend to shift the optimal generalization to the underparametrized regime: (i) increasing the numbers of learners from which we average the predictions,  $K$ , (ii) decreasing the signal-to-noise ratio (SNR),  $F/\tau$ , and (iii) decreasing the size of the dataset,  $N/D$ . In other words, when ensembling on a small, noisy dataset, one is better off using an underparametrized model.

These three effects are shown in figure 12. In the left panel, we see that as we increase  $K$ , the minimum of generalization error jumps to the underparametrized regime  $P < N$  for a high enough value of  $K$ . In the central/right panels, a similar effect occurs when decreasing the SNR or decreasing  $N/D$ .

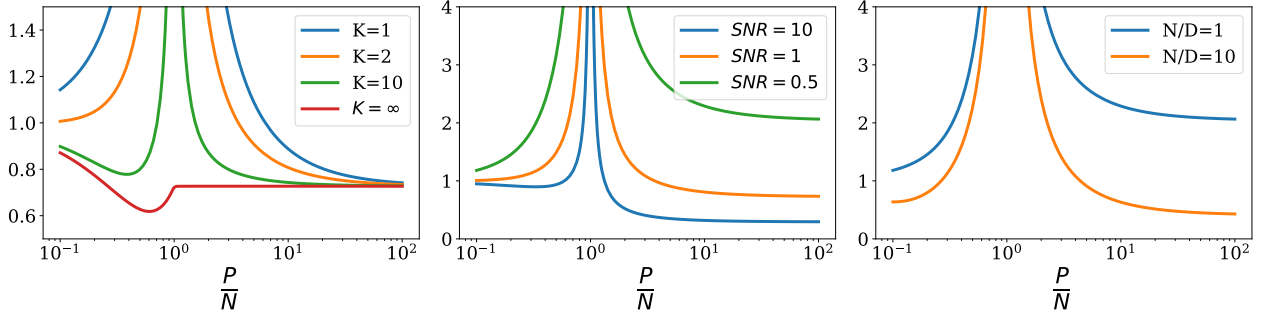


Figure 12: Generalisation error as a function of  $P/N$ : depending on the values of  $K$ ,  $F/\tau$  and  $N/D$ , optimal generalization can be reached in the underparametrized regime or the overparametrized regime. **Left:**  $F/\tau = 1$ ,  $N/D = 1$  and we vary  $K$ . This is the same as figure 5 in the main text, except that the higher noise causes the ensembling curve at  $K \rightarrow \infty$  to exhibit a *dip* in the underparametrized regime. **Center:**  $K = 2$ ,  $N/D = 1$  and we vary  $F/\tau$ . **Right:**  $F/\tau = 1$ ,  $K = 2$  and we vary  $N/D$ .

## B Statement of the Main Result

### B.1 Assumptions

First, we state precisely the assumptions under which our main result is valid. Note, that these are the same as in [11].

**Assumption 1:**  $\sigma : \mathbb{R} \rightarrow \mathbb{R}$  is a weakly differential function with derivative  $\sigma'$ . Assume there exists  $c_0, c_1 < \infty \in \mathbb{R}$  such that for all  $u \in \mathbb{R}$   $|\sigma(u)|, |\sigma'(u)| \leq c_0 e^{c_1|u|}$ . Then define:

$$\mu_0 = \mathbb{E}[\sigma(u)] \quad \mu_1 = \mathbb{E}[u\sigma(u)] \quad \mu_*^2 = \mathbb{E}[\sigma^2(u)] - \mu_0^2 - \mu_1^2, \quad (29)$$

where the expectation is over  $u \sim \mathcal{N}(0, 1)$ . To facilitate readability, we specialize to the case  $\mu_0 = 0$ . This simply amounts to a shift ctivation function  $\tilde{\sigma}$  of the network,  $\tilde{\sigma}(x) = \sigma(x) - \mu_0$ .

**Assumption 2:** We work in the high-dimensional limit, i.e. in the limit where the input dimension  $D$ , the hidden layer dimension  $P$  and the number of training points  $N$  go to infinity with their ratios fixed. That is:

$$N, P, D \rightarrow \infty, \quad \frac{P}{D} \equiv \psi_1 = \mathcal{O}(1), \quad \frac{N}{D} \equiv \psi_2 = \mathcal{O}(1). \quad (30)$$

This condition implies that, in the computation of the risk  $\mathcal{R}$ , we can neglect all the terms of order  $\mathcal{O}(1)$  in favour of the terms of order  $\mathcal{O}(D)$ .

**Assumption 3:** The labels are given by a linear ground truth, or teacher function:

$$y_\mu = f_d(\mathbf{X}_\mu) + \epsilon_\mu, \quad f_d(\mathbf{x}) = \langle \boldsymbol{\beta}, \mathbf{x} \rangle, \quad \|\boldsymbol{\beta}\| = F, \quad \epsilon_\mu \sim \mathcal{N}(0, \tau). \quad (31)$$

Note that as explained in [11], it is easy to add a non linear component to the teacher, but the latter would not be captured by the model (the student) in the regime  $N/D = \mathcal{O}(1)$ , and would simply amount to an extra noise term.

## B.2 Results

Here we give the explicit form of the quantities appearing in our main result. In these expressions, the index  $a \in \{v, e, d\}$  distinguishes the *vanilla*, *ensembling* and *divide and conquer* terms.

$$\begin{aligned} \Psi_1 &= \frac{1}{D} \text{Tr} \left[ H[S^v]^{-1} H[P_{\Psi_1}] \right], \\ \Psi_2^v &= \frac{1}{D} \text{Tr} \left[ H[S^v]^{-1} H[P_{\Psi_2^v}] \right], \\ \Psi_3^v &= \frac{1}{D} \text{Tr} \left[ H[S^v]^{-1} H[P_{\Psi_3^v}] \right], \\ \Psi_2^e &= \frac{1}{D} \text{Tr} \left[ H[S^e]^{-1} H[P_{\Psi_2^e}] \right], \\ \Psi_3^e &= \frac{1}{D} \text{Tr} \left[ H[S^e]^{-1} H[P_{\Psi_3^e}] \right], \\ \Psi_2^d &= \frac{1}{D} \text{Tr} \left[ H[S^d]^{-1} H[P_{\Psi_2^d}] \right], \end{aligned}$$

where the Hessian matrix  $H[F]$ , for a given function  $F : (q, r, \tilde{q}, \tilde{r}) \mapsto \mathbb{R}$  is defined as:

$$H[F] = \begin{bmatrix} \frac{\partial F}{\partial q \partial q} & \frac{\partial F}{\partial q \partial r} & \frac{\partial F}{\partial q \partial \tilde{q}} & \frac{\partial F}{\partial q \partial \tilde{r}} \\ \frac{\partial F}{\partial r \partial q} & \frac{\partial F}{\partial r \partial r} & \frac{\partial F}{\partial r \partial \tilde{q}} & \frac{\partial F}{\partial r \partial \tilde{r}} \\ \frac{\partial F}{\partial \tilde{q} \partial q} & \frac{\partial F}{\partial \tilde{q} \partial r} & \frac{\partial F}{\partial \tilde{q} \partial \tilde{q}} & \frac{\partial F}{\partial \tilde{q} \partial \tilde{r}} \\ \frac{\partial F}{\partial \tilde{r} \partial q} & \frac{\partial F}{\partial \tilde{r} \partial r} & \frac{\partial F}{\partial \tilde{r} \partial \tilde{q}} & \frac{\partial F}{\partial \tilde{r} \partial \tilde{r}} \end{bmatrix} \bigg|_{\substack{q=q^* \\ r=r^* \\ \tilde{r}=0 \\ \tilde{q}=0}},$$

with  $q^*$  and  $r^*$  being the solutions of the fixed point equation for the function  $S_0 : (q, r) \mapsto \mathbb{R}$  defined below:

$$\begin{cases} \frac{\partial S_0(q, r)}{\partial q} = 0 \\ \frac{\partial S_0(q, r)}{\partial r} = 0. \end{cases}$$

$$S_0(q, r) = \lambda \psi_1^2 \psi_2 q + \psi_2 \log \left( \frac{\mu_1^2 \psi_1 q}{\mu_1^2 \psi_1 r + 1} + 1 \right) + \frac{r}{q} + (1 - \psi_1) \log(q) + \psi_2 \log(\mu_1^2 \psi_1 r + 1) - \log(r).$$

The explicit expression of the above quantities in terms of  $(q, r, \tilde{q}, \tilde{r})$  is given below.

## B.3 Explicit expression of $S^v, S^e, S^d$

Here we present the explicit formulas for  $S^v, S^e, S^d$ , which are defined as the functions  $(q, r, \tilde{q}, \tilde{r}) \mapsto \mathbb{R}$  such that:

$$\begin{aligned} S^v(q, r, \tilde{q}, \tilde{r}) &= 2(S_0(q, r) + \tilde{q} f^v(q, r) + \tilde{r} g^v(q, r)) \\ S^e(q, r, \tilde{q}, \tilde{r}) &= S_0(q, r) + \tilde{r}^2 f^e(q, r) + \tilde{q}^2 g^e(q, r) \\ S^d(q, r, \tilde{q}, \tilde{r}) &= S_0(q, r) + \tilde{r}^2 f^d(q, r) + \tilde{q}^2 g^d(q, r), \end{aligned}$$

where we defined the functions  $(q, r) \mapsto \mathbb{R}$ ,

$$\begin{aligned}
f^v(q, r) &= \lambda \psi_1^2 \psi_2 + \frac{\mu_\star^2 \psi_1 \psi_2}{\mu_\star^2 \psi_1 q + \mu_1^2 \psi_1 r + 1} + \frac{1 - \psi_1}{q} - \frac{r}{q^2}, \\
g^v(q, r) &= -\frac{\mu_\star^2 \mu_1^2 \psi_1^2 \psi_2 q}{(\mu_1^2 \psi_1 r + 1)(\mu_\star^2 \psi_1 q + \mu_1^2 \psi_1 r + 1)} + \frac{\mu_1^2 \psi_1 \psi_2}{\mu_1^2 \psi_1 r + 1} + \frac{1}{q} - \frac{1}{r}, \\
f^e(q, r) &= \frac{2r \mu_1^2 \psi_1 (1 + q \mu_\star^2 \psi_1) + (1 + q \mu_\star^2 \psi_1)^2 - r^2 \mu_1^4 \psi_1^2 (-1 + \psi_2)}{r^2 (1 + r \mu_1^2 \psi_1 + q \mu_\star^2 \psi_1)^2}, \\
g^e(q, r) &= \frac{\psi_1}{q^2}, \\
f^d(q, r) &= \frac{1}{r^2}, \\
g^d(q, r) &= \frac{\psi_1}{q^2}.
\end{aligned}$$

#### B.4 Explicit expression of $P_{\Psi_1}, P_{\Psi_2}^v, P_{\Psi_3}^v, P_{\Psi_2}^e, P_{\Psi_3}^e, P_{\Psi_2}^d$

Here we present the explicit formulas for  $P_{\Psi_1}, P_{\Psi_2}^v, P_{\Psi_3}^v, P_{\Psi_2}^e, P_{\Psi_3}^e, P_{\Psi_2}^d$ , which are defined as the functions  $(q, r, \tilde{q}, \tilde{r}) \mapsto \mathbb{R}$  such that:

$$\begin{aligned}
P_{\Psi_1} &= \psi_1 \psi_2 \mu_1^2 \left( M_X^{11} + \mu_1^2 \mu_\star^2 \psi_1^2 (M_X M_W^v M_X)^{11} + \mu_\star^2 \psi_1 (M_X M_W^v)^{11} \right), \\
P_{\Psi_2^v} &= D \psi_1^2 \psi_2 (\mu_1^2 \tilde{r} + \mu_\star^2 \tilde{q}) \left[ \mu_1^2 P_{XX}^v - 2 \mu_1^2 \mu_\star^2 \psi_1 P_{WX}^v + \mu_\star^2 P_{WW}^v \right], \\
P_{\Psi_3^v} &= D \psi_1^2 \psi_2 (\mu_1^2 \tilde{r} + \mu_\star^2 \tilde{q}) \left[ \mu_1^2 \left( M_X^{12} + \mu_1^2 \mu_\star^2 \psi_1^2 [M_X M_W^v M_X]^{12} \right) - 2 \mu_1^2 \mu_\star^2 \psi_1 [M_X M_W^v]^{12} + \mu_\star^2 [M_W^v]^{12} \right], \\
P_{\Psi_2^e} &= D \psi_1^2 \psi_2 \mu_1^2 \tilde{r} \left[ \mu_1^2 P_{XX}^e - 2 \mu_1^2 \mu_\star^2 \psi_1 P_{WX}^e + \mu_\star^2 P_{WW}^e \right], \\
P_{\Psi_3^e} &= D \psi_1^2 \psi_2 \mu_1^2 \tilde{r} \left[ \mu_1^2 \left( M_X^{12} + \mu_1^2 \mu_\star^2 \psi_1^2 [M_X M_W^e M_X]^{12} \right) - 2 \mu_1^2 \mu_\star^2 \psi_1 [M_X M_W^e]^{12} + \mu_\star^2 [M_W^e]^{12} \right], \\
P_{\Psi_2^d} &= D \mu_1^2 \psi_1 \psi_2^2 \tilde{r} \left[ \psi_1 \mu_1^2 P_{XX} + 2 \mu_\star^2 \mu_1^2 \psi_1^2 P_{WX} + \mu_\star^2 \psi_1 P_{WW} \right],
\end{aligned}$$

where we defined the scalars  $P_{XX}, P_{WX}, P_{WW}$  as follows:

$$\begin{aligned}
P_{XX}^v &= \psi_2 N_X^{12} + M_X^{12} + 2 \psi_2 (\mu_1 \mu_\star \psi_1)^2 [M_X N_X M_W^a]^{12} + (\mu_1 \mu_\star \psi_1)^2 [M_X M_W^a M_X]^{12} \\
&\quad + \psi_2 (\mu_1 \mu_\star \psi_1)^4 [M_X M_W N_X M_W^a M_X]^{12}, \\
P_{WX}^v &= \psi_2 [N_X M_W^a]^{12} + [M_X M_W^a]^{12} + \psi_2 (\mu_1 \mu_\star \psi_1)^2 [M_X M_W^a N_X M_W^a]^{12}, \\
P_{WW}^v &= [M_W^a]^{12} + \psi_2 (\mu_1 \mu_\star \psi_1)^2 [M_W^a N_X M_W^a]^{12}, \\
P_{XX}^e &= P_{XX}^v, \\
P_{WX}^e &= P_{WX}^v, \\
P_{WW}^e &= P_{WW}^v, \\
P_{XX}^d &= \left( N_X^{d11} + 2 (\mu_1 \mu_\star \psi_1)^2 [N_X^d M_W^d M_X^d]^{11} + (\mu_1 \mu_\star \psi_1)^4 [M_X^d M_W^d N_X^d M_W^d M_X^d]^{11} \right), \\
P_{WX}^d &= [N_X^d M_W^d]^{11} + (\mu_1 \mu_\star \psi_1)^2 [M_X^d M_W^d N_X^d M_W^d]^{11}, \\
P_{WW}^d &= (\mu_1 \mu_\star \psi_1)^2 [M_W^d N_X^d M_W^d]^{11},
\end{aligned}$$

and the  $2 \times 2$  matrices  $M_X, M_W, N_X$  as follows:

$$\begin{aligned}
M_X^v &= \begin{bmatrix} \frac{r}{1 + \mu_1^2 \psi_1 r} & \frac{\tilde{r}}{(1 + \mu_1^2 \psi_1 r)^2} \\ \frac{\tilde{r}}{(1 + \mu_1^2 \psi_1 r)^2} & \frac{r}{1 + \mu_1^2 \psi_1 r} \end{bmatrix}, \quad M_W^v = \begin{bmatrix} \frac{q(1 + \mu_1^2 \psi_1 r)}{1 + 2 \mu_1^2 \psi_1 r + \mu_\star^2 \psi_1 q} & \frac{q^2 \mu_1^2 \mu_\star^2 \psi_1^2 \tilde{r}}{(1 + \mu_1^2 \psi_1 r + \mu_\star^2 \psi_1 q)^2} \\ \frac{q^2 \mu_1^2 \mu_\star^2 \psi_1^2 \tilde{r}}{(1 + \mu_1^2 \psi_1 r + \mu_\star^2 \psi_1 q)^2} & \frac{q(1 + \mu_1^2 \psi_1 r)}{1 + 2 \mu_1^2 \psi_1 r + \mu_\star^2 \psi_1 q} \end{bmatrix}, \quad N_X^v = \frac{1}{(1 + \mu_1^2 \psi_1 r)^2} \begin{bmatrix} r & \tilde{r} \\ \tilde{r} & r \end{bmatrix}, \\
M_X^e &= M_X^v, \quad M_W^e = M_W^v + \frac{(1 + r \mu_1^2 \psi_1)^2 \tilde{q}}{(1 + \mu_1^2 \psi_1 r + \mu_\star^2 \psi_1 q)^2} \begin{bmatrix} 0 & 1 \\ 1 & 0 \end{bmatrix}, \quad N_X^e = \frac{1}{(1 + \mu_1^2 \psi_1 r)^2} \begin{bmatrix} r & \tilde{r} \\ \tilde{r} & r \end{bmatrix}, \\
M_X^d &= \frac{r}{1 + \mu_1^2 \psi_1 r^2} \begin{bmatrix} 1 & 0 \\ 0 & 1 \end{bmatrix}, \quad M_W^d = \frac{q(1 + \mu_1^2 \psi_1 r)}{1 + \mu_1^2 \psi_1 r + \mu_\star^2 \psi_1 q} \begin{bmatrix} 1 & 0 \\ 0 & 1 \end{bmatrix}, \quad N_X^d = \frac{1}{(1 + \mu_1^2 \psi_1 r)^2} \begin{bmatrix} \tilde{r} & 0 \\ 0 & \tilde{r} \end{bmatrix}.
\end{aligned}$$

## C Replica Computation

### C.1 Toolkit

#### C.1.1 Gaussian integrals

In order to obtain the main result for the generalisation error, we perform the averages over all the sources of randomness in the system in the following order: over the dataset  $X$ , then over the noise  $W$ , and finally over the random feature layers  $\Theta$ . Here are some useful formulae used throughout the computations:

$$\begin{cases} \int e^{-\frac{1}{2}x_i G_{ij} x_j + J_i x_i} dx & = (\det G)^{-\frac{1}{2}} e^{\frac{1}{2}J_i G_{ij}^{-1} J_j}, \\ \int x_a e^{-\frac{1}{2}x_i G_{ij} x_j + J_i x_i} dx & = P_a^1 (\det G)^{-\frac{1}{2}} e^{\frac{1}{2}J_i G_{ij}^{-1} J_j}, \\ \int x_a x_b e^{-\frac{1}{2}x_i G_{ij} x_j + J_i x_i} dx & = P_{ab}^2 (\det G)^{-\frac{1}{2}} e^{\frac{1}{2}J_i G_{ij}^{-1} J_j}, \\ \int x_a x_b x_c e^{-\frac{1}{2}x_i G_{ij} x_j + J_i x_i} dx & = P_{abc}^3 (\det G)^{-\frac{1}{2}} e^{\frac{1}{2}J_i G_{ij}^{-1} J_j}, \\ \int x_a x_b x_c x_d e^{-\frac{1}{2}x_i G_{ij} x_j + J_i x_i} dx & = P_{abcd}^4 (\det G)^{-\frac{1}{2}} e^{\frac{1}{2}J_i G_{ij}^{-1} J_j}, \end{cases} \quad (32)$$

with

$$\begin{aligned} P_a^1 &= [G^{-1}J]_a, \\ P_{ab}^2 &= ((G^{-1})_{ab} + [G^{-1}J]_a [G^{-1}J]_b), \\ P_{abc}^3 &= \sum_{\bar{a}, \bar{b}, \bar{c} \in \text{perm}(abc)} ((G^{-1})_{\bar{a}\bar{b}} [G^{-1}J]_{\bar{c}} + [G^{-1}J]_{\bar{a}} [G^{-1}J]_{\bar{b}} [G^{-1}J]_{\bar{c}}), \\ P_{abcd}^4 &= \sum_{\bar{a}, \bar{b}, \bar{c}, \bar{d} \in \text{perm}(abcd)} \left( (G^{-1})_{\bar{a}\bar{b}} (G^{-1})_{\bar{c}\bar{d}} + [G^{-1}J]_{\bar{a}} [G^{-1}J]_{\bar{b}} [G^{-1}J]_{\bar{c}} [G^{-1}J]_{\bar{d}} + (G^{-1})_{\bar{a}\bar{b}} [G^{-1}J]_{\bar{c}} [G^{-1}J]_{\bar{d}} \right). \end{aligned}$$

#### C.1.2 Replica representation of an inverse matrix

To obtain gaussian integrals we will use the "replica" representation the element  $(ij)$  of a matrix  $M$  of size  $D$ :

$$M_{ij}^{-1} = \lim_{n \rightarrow 0} \int \left( \prod_{\alpha=1}^n \prod_{i=1}^D d\eta_i^\alpha \right) \eta_i^1 \eta_j^1 \exp \left( -\frac{1}{2} \eta_i^\alpha M_{ij} \eta_j^\alpha \right). \quad (33)$$

Indeed, using the gaussian integral representation of the inverse of  $M$ ,

$$\begin{aligned} M_{ij}^{-1} &= \mathcal{Z}^{-1} \int \left( \prod_{i=1}^D d\eta_i \right) \eta_i \eta_j \exp \left( -\frac{1}{2} \eta_i M_{ij} \eta_j \right), \\ \mathcal{Z} &= \sqrt{\frac{2\pi}{\det M}} \\ &= \int \left( \prod_{i=1}^D d\eta_i \right) \exp \left( -\frac{1}{2} \eta_i M_{ij} \eta_j \right). \end{aligned}$$

Using the replica identity, we rewrite this as

$$M_{ij}^{-1} = \lim_{n \rightarrow 0} \mathcal{Z}^{n-1} \int \left( \prod_{i=1}^D d\eta_i \right) \eta_i \eta_j \exp \left( -\frac{1}{2} \eta_i M_{ij} \eta_j \right).$$

Renaming the integration variable of the integral on the left as  $\eta^1$  and the  $n-1$  others as  $\eta^\alpha, \alpha \in \{2, n\}$ , we obtain expression (33).

### C.2 The Random Feature model

In what follows, we will explicitly leave the indices of all the quantities used. We use the notation, called Einstein summation convention in physics, in which all repeated indices are summed but the sum is not explicitly written. Indices  $i \in \{1 \dots D\}$  are used to refer to the input dimension,  $h \in \{1 \dots P\}$  to refer to the hidden layer dimension and  $\mu \in \{1 \dots N\}$  to refer to the number of data points.

### C.2.1 With a single learner

In the random features model, the predictor can be computed explicitly:

$$f(\mathbf{x}) = \mathbf{y}_\mu^\top \mathbf{Z}_{\mu h} (\mathbf{Z}^\top \mathbf{Z} + \psi_1 \psi_2 \lambda \mathbf{I}_N)_{hh'}^{-1} \sigma \left( \frac{\boldsymbol{\Theta}_{h'i} \mathbf{x}_i}{\sqrt{D}} \right) / \sqrt{D}, \quad (34)$$

where

$$\mathbf{y}_\mu = f_d(\mathbf{X}_\mu) + \boldsymbol{\epsilon}_\mu, \quad (35)$$

$$\mathbf{Z}_{\mu h} = \frac{1}{\sqrt{D}} \sigma \left( \frac{1}{\sqrt{D}} \boldsymbol{\Theta}_{hi} \mathbf{X}_{\mu i} \right). \quad (36)$$

Hence the generalization error can be computed as:

$$\mathcal{R}_{\text{RF}} = \mathbb{E}_{\mathbf{x}} \left[ \left( f_d(\mathbf{x}) - \mathbf{y}_\mu^\top \mathbf{Z}_{\mu h} (\mathbf{Z}^\top \mathbf{Z} + \psi_1 \psi_2 \lambda \mathbf{I}_N)_{hh'}^{-1} \sigma \left( \frac{\boldsymbol{\Theta}_{h'i} \mathbf{x}_i}{\sqrt{D}} \right) / \sqrt{D} \right)^2 \right] \quad (37)$$

$$\begin{aligned} &= \mathbb{E}_{\mathbf{x}} [f_d(\mathbf{x})^2] - 2 \mathbf{y}_\mu^\top \mathbf{Z}_{\mu h} (\mathbf{Z}^\top \mathbf{Z} + \psi_1 \psi_2 \lambda \mathbf{I}_N)_{hh'}^{-1} \mathbf{V}_{h'} / \sqrt{D} \\ &\quad + \mathbf{y}_\mu^\top \mathbf{Z}_{\mu h} (\mathbf{Z}^\top \mathbf{Z} + \psi_1 \psi_2 \lambda \mathbf{I}_N)_{hh_1}^{-1} \mathbf{U}_{h_1 h_2} (\mathbf{Z}^\top \mathbf{Z} + \psi_1 \psi_2 \lambda \mathbf{I}_N)_{h_2 h'}^{-1} \mathbf{Z}_{h' \mu'}^\top \mathbf{y}_{\mu'} / D, \end{aligned} \quad (38)$$

where

$$\mathbf{V}_h = \mathbb{E}_{\mathbf{x}} \left[ f_d(\mathbf{x}) \sigma \left( \frac{\langle \boldsymbol{\Theta}_{hi} \mathbf{x}_i \rangle}{\sqrt{D}} \right) \right], \quad (39)$$

$$\mathbf{U}_{hh'} = \mathbb{E}_{\mathbf{x}} \left[ \sigma \left( \frac{\langle \boldsymbol{\Theta}_{hi} \mathbf{x}_i \rangle}{\sqrt{D}} \right) \sigma \left( \frac{\langle \boldsymbol{\Theta}_{h'i} \mathbf{x}_i \rangle}{\sqrt{D}} \right) \right]. \quad (40)$$

### C.2.2 Ensembling over $K$ learners

When ensembling over  $K$  learners with independently sampled random feature vectors, the predictor becomes:

$$f(\mathbf{x}) = \frac{1}{K\sqrt{D}} \sum_k \mathbf{y}_\mu^\top \mathbf{Z}_{\mu h}^{(k)} \left( \mathbf{Z}^{\text{T}(k)} \mathbf{Z}^{(k)} + \psi_1 \psi_2 \lambda \mathbf{I}_N \right)_{hh'}^{-1} \sigma \left( \frac{\boldsymbol{\Theta}_{h'i}^{(k)} \mathbf{x}_i}{\sqrt{D}} \right), \quad (41)$$

where

$$\mathbf{Z}_{\mu h}^{(k)} = \frac{1}{\sqrt{D}} \sigma \left( \frac{1}{\sqrt{D}} \boldsymbol{\Theta}_{hi}^{(k)} \mathbf{X}_{\mu i} \right). \quad (42)$$

The generalisation error is then given by:

$$\mathcal{R}_{\text{RF}} = \mathbb{E}_{\mathbf{x}} \left[ \left( f_d(\mathbf{x}) - \frac{1}{K} \sum_k \mathbf{y}^\top \mathbf{Z}^{(k)} \left( \mathbf{Z}^{\text{T}(k)} \mathbf{Z}^{(k)} + \psi_1 \psi_2 \lambda \mathbf{I}_N \right)^{-1} \sigma \left( \frac{\boldsymbol{\Theta}_{h'i}^{(k)} \mathbf{x}_i}{\sqrt{D}} \right) / \sqrt{D} \right)^2 \right] \quad (43)$$

$$\begin{aligned} &= \mathbb{E}_{\mathbf{x}} [f_d(\mathbf{x})^2] - \frac{2}{K} \sum_k \mathbf{y}^\top \mathbf{Z}^{(k)} \left( \mathbf{Z}^{\text{T}(k)} \mathbf{Z}^{(k)} + \psi_1 \psi_2 \lambda \mathbf{I}_N \right)^{-1} \mathbf{V}^{(k)} / \sqrt{D} \\ &\quad + \frac{1}{K^2} \sum_{\substack{k \\ l \neq k}} \mathbf{y}^\top \mathbf{Z}^{(k)} \left( \mathbf{Z}^{\text{T}(k)} \mathbf{Z}^{(k)} + \psi_1 \psi_2 \lambda \mathbf{I}_N \right)^{-1} \mathbf{U}^{(kl)} \left( \mathbf{Z}^{\text{T}(l)} \mathbf{Z}^{(l)} + \psi_1 \psi_2 \lambda \mathbf{I}_N \right)^{-1} \mathbf{Z}^{(l)\top} \mathbf{T} \mathbf{y} / D, \end{aligned} \quad (44)$$

where

$$\mathbf{V}_h^{(k)} = \mathbb{E}_{\mathbf{x}} \left[ f_d(\mathbf{x}) \sigma \left( \frac{\langle \boldsymbol{\Theta}_{hi}^{(k)} \mathbf{x}_i \rangle}{\sqrt{D}} \right) \right], \quad (45)$$

$$\mathbf{U}_{hh'}^{(kl)} = \mathbb{E}_{\mathbf{x}} \left[ \sigma \left( \frac{\langle \boldsymbol{\Theta}_{hi}^{(k)} \mathbf{x}_i \rangle}{\sqrt{D}} \right) \sigma \left( \frac{\langle \boldsymbol{\Theta}_{h'i}^{(l)} \mathbf{x}_i \rangle}{\sqrt{D}} \right) \right]. \quad (46)$$

### C.2.3 Equivalent Gaussian Covariate Model

It was shown in [11] that the random features model is equivalent, in the high-dimensional limit of Assumption 2, to a Gaussian covariate model in which the activation function  $\sigma$  is replaced as:

$$\sigma\left(\frac{\Theta_{hi}^{(k)} \mathbf{X}_{\mu i}}{\sqrt{D}}\right) \rightarrow \mu_0 + \mu_1 \frac{\Theta_{hi}^{(k)} \mathbf{X}_{\mu i}}{\sqrt{D}} + \mu_\star \mathbf{W}_{\mu h}^{(k)}, \quad (47)$$

with  $\mathbf{W}^{(k)} \in \mathbb{R}^{N \times P}$ ,  $W_{\mu h}^{(k)} \sim \mathcal{N}(0, 1)$  and  $\mu_0$ ,  $\mu_1$  and  $\mu_\star$  defined in (29). To simplify the calculations, we take  $\mu_0 = 0$ , which amounts to adding a constant term to the activation function  $\sigma$ .

This powerful mapping allows to express the quantities  $\mathbf{U}$ ,  $\mathbf{V}$ . We will not repeat their calculations here: the only difference here is  $\mathbf{U}^{kl}$ , which carries extra indices  $k, l$  due to the different initialization of the random features  $\Theta^{(k)}$ . In our case,

$$\mathbf{U}_{hh'}^{(kl)} = \frac{\mu_1^2}{D} \Theta_{hi}^{(k)} \Theta_{h'i}^{(l)} + \mu_\star^2 \delta_{kl} \delta_{hh'}. \quad (48)$$

Hence we can rewrite the generalization error as

$$\mathbb{E}_{\{\Theta^{(k)}\}, \mathbf{X}, \epsilon} [\mathcal{R}_{\text{RF}}] = F^2 (1 - 2\Psi_1^v) + \frac{1}{K} (F^2 \Psi_2^v + \tau^2 \Psi_3^v) + \left(1 - \frac{1}{K}\right) (F^2 \Psi_2^e + \tau^2 \Psi_3^e), \quad (49)$$

where  $\Psi_1, \Psi_2^v, \Psi_2^e, \Psi_3^v, \Psi_3^e$  are given by:

$$\begin{aligned} \Psi_1 &= \frac{1}{d} \text{Tr} \left[ \left( \frac{\mu_1}{d} \mathbf{X} \Theta^{(1)\top} \right)^\top \mathbf{Z}^{(1)} \left( \mathbf{Z}^{(1)\top} \mathbf{Z}^{(1)} + \psi_1 \psi_2 \lambda \mathbf{I}_N \right)^{-1} \right], \\ \Psi_2^v &= \frac{1}{d} \text{Tr} \left[ \left( \mathbf{Z}^{(1)\top} \mathbf{Z}^{(1)} + \psi_1 \psi_2 \lambda \mathbf{I}_N \right)^{-1} \left( \frac{\mu_1^2}{d} \Theta^{(1)} \Theta^{(1)\top} + \mu_\star^2 \mathbf{I}_N \right) \left( \mathbf{Z}^{(1)\top} \mathbf{Z}^{(1)} + \psi_1 \psi_2 \lambda \mathbf{I}_N \right)^{-1} \mathbf{Z}^{(1)\top} \left( \frac{1}{d} \mathbf{X} \mathbf{X}^\top \right) \mathbf{Z}^{(1)} \right], \\ \Psi_3^v &= \frac{1}{d} \text{Tr} \left[ \left( \mathbf{Z}^{(1)\top} \mathbf{Z}^{(1)} + \psi_1 \psi_2 \lambda \mathbf{I}_N \right)^{-1} \left( \frac{\mu_1^2}{d} \Theta^{(1)} \Theta^{(1)\top} + \mu_\star^2 \mathbf{I}_N \right) \left( \mathbf{Z}^{(1)\top} \mathbf{Z}^{(1)} + \psi_1 \psi_2 \lambda \mathbf{I}_N \right)^{-1} \mathbf{Z}^{(1)\top} \mathbf{Z}^{(1)} \right], \\ \Psi_2^e &= \frac{1}{d} \text{Tr} \left[ \left( \mathbf{Z}^{(1)\top} \mathbf{Z}^{(1)} + \psi_1 \psi_2 \lambda \mathbf{I}_N \right)^{-1} \left( \frac{\mu_1^2}{d} \Theta^{(1)} \Theta^{(2)\top} \right) \left( \mathbf{Z}^{(2)\top} \mathbf{Z}^{(2)} + \psi_1 \psi_2 \lambda \mathbf{I}_N \right)^{-1} \mathbf{Z}^{(2)\top} \left( \frac{1}{d} \mathbf{X} \mathbf{X}^\top \right) \mathbf{Z}^{(1)} \right], \\ \Psi_3^e &= \frac{1}{d} \text{Tr} \left[ \left( \mathbf{Z}^{(1)\top} \mathbf{Z}^{(1)} + \psi_1 \psi_2 \lambda \mathbf{I}_N \right)^{-1} \left( \frac{\mu_1^2}{d} \Theta^{(1)} \Theta^{(2)\top} \right) \left( \mathbf{Z}^{(2)\top} \mathbf{Z}^{(2)} + \psi_1 \psi_2 \lambda \mathbf{I}_N \right)^{-1} \mathbf{Z}^{(2)\top} \mathbf{Z}^{(1)} \right]. \end{aligned}$$

### C.3 Computation of the *vanilla* terms

To start with, let us compute the vanilla terms (those who carry a superscript  $v$ ), which involve a single instance of the random feature vectors. Note that these were calculated in [11] by evaluating the Stieljes transform of the random matrices of which we need to calculate the trace. The replica method used here makes the calculation of the vanilla terms carry over easily to the the ensembling terms (superscript  $e$ ) and the divide and conquer term (superscript  $d$ ). To illustrate the calculation steps, we will calculate  $\Psi_3^v$ , then provide the results for  $\Psi_2^v$  and  $\Psi_1$ . In the vanilla terms, the two inverse matrices that appear are the same. Hence we use twice the replica identity (33), introducing  $2n$  replicas which all play the same role:

$$M_{ij}^{-1} M_{kl}^{-1} = \lim_{n \rightarrow 0} \int \left( \prod_{\alpha=1}^{2n} d\eta \right) \eta_i^1 \eta_j^1 \eta_k^2 \eta_l^2 \exp \left( -\frac{1}{2} \eta^\alpha M_{ij} \eta^\alpha \right). \quad (50)$$

The first step is to perform the averages, i.e. the Gaussian integrals, over the dataset  $\mathbf{X}$ , the deterministic noise  $\mathbf{W}$  induced by the non-linearity of the activation function and the random features  $\Theta$ .

### C.3.1 Averaging over the dataset

Replacing the activation function by its Gaussian covariate equivalent model and using (50), the term  $\Psi_3$  can be expanded as:

$$\begin{aligned}\Psi_3^v &= \frac{1}{D} \left[ Z_{\mu h} (Z^\top Z + \psi_1 \psi_2 \lambda \mathbf{I}_N)_{hh_1}^{-1} \left( \frac{\mu_1^2}{D} \Theta_{h_1 i} \Theta_{h_2 i} + \mu_\star^2 \delta_{h_1 h_2} \right) (Z^\top Z + \psi_1 \psi_2 \lambda \mathbf{I}_N)_{h_2 h'}^{-1} Z_{h' \mu} \right] \\ &= \frac{1}{D} \left( \frac{\mu_1^2}{D} \Theta_{h_1 i} \Theta_{h_2 i} + \mu_\star^2 \delta_{h_1 h_2} \right) [Z_{\mu h} Z_{h' \mu}] \int \left( \prod_{\alpha=1}^{2n} d\eta^\alpha \right) \eta_h^1 \eta_{h_1}^1 \eta_{h_2}^2 \eta_{h'}^2 \exp \left( -\frac{1}{2} \eta_h^\alpha (Z^\top Z + \psi_1 \psi_2 \lambda \mathbf{I}_N)_{hh'} \eta_{h'}^\alpha \right) \\ &= \frac{1}{D^2} \left( \frac{\mu_1^2}{D} \Theta_{h_1 i} \Theta_{h_2 i} + \mu_\star^2 \delta_{h_1 h_2} \right) \left( \frac{\mu_1}{\sqrt{D}} \Theta X + \mu_\star W \right)_{h\mu} \left( \frac{\mu_1}{\sqrt{D}} \Theta X + \mu_\star W \right)_{h'\mu} \\ &\quad \int \left( \prod_{\alpha=1}^{2n} d\eta^\alpha \right) \eta_h^1 \eta_{h_1}^1 \eta_{h_2}^2 \eta_{h'}^2 \exp \left( -\frac{1}{2} \eta_h^\alpha \left( \frac{1}{D} \left( \frac{\mu_1}{\sqrt{D}} \Theta X + \mu_\star W \right)_{h\mu} \left( \frac{\mu_1}{\sqrt{D}} \Theta X + \mu_\star W \right)_{h'\mu} + \psi_1 \psi_2 \lambda \delta_{hh'} \right) \eta_{h'}^\alpha \right).\end{aligned}$$

Now, we introduce  $\lambda_i := \frac{1}{\sqrt{P}} \eta_h \Theta_{hi}$ , and enforce this relation using the integral representation of a delta-function:

$$1 = \int d\lambda_i^\alpha d\hat{\lambda}_i^\alpha e^{i\hat{\lambda}_i^\alpha (\sqrt{P}\lambda_i^\alpha - \eta_h^\alpha \Theta_{hi})}. \quad (51)$$

The average over the dataset  $X_{\mu i}$  has the form of (32) with:

$$(G_X)_{\mu\mu', ii'} = \delta_{\mu\mu'} \left( \delta_{ii'} + \frac{\mu_1^2 \psi_1}{D} \lambda_i^\alpha \lambda_{i'}^\alpha \right), \quad (52)$$

$$(J_X)_{\mu, i} = \frac{\mu_1 \mu_\star \sqrt{\psi_1}}{D} \sum_{\alpha} \lambda_i^\alpha \eta_h^\alpha W_{\mu h}. \quad (53)$$

Using formulae (32), we obtain:

$$\begin{aligned}\Psi_3^v &= \frac{N}{D^2} \int \left( \prod_{\alpha=1}^{2n} d\eta^\alpha d\lambda^\alpha d\hat{\lambda}^\alpha \right) \left( \frac{\mu_1^2 P}{D} \lambda_i^1 \lambda_i^2 + \mu_\star^2 \eta_i^1 \eta_i^2 \right) \\ &\quad \left[ \mu_\star^2 \eta_h^1 W_h W_{h'} \eta_{h'}^2 + \mu_1^2 \psi_1 \lambda_i^1 \lambda_{i'}^2 ((G_X^{-1})_{ii'} + (G_X^{-1} J_X)_i (G_X^{-1} J_X)_{i'}) + 2\mu_1 \mu_\star \sqrt{\psi_1} \lambda_i^1 W_h \eta_h^2 (G_X^{-1} J_X)_i \right] \\ &\quad \exp \left( -\frac{n}{2} \log \det(G_X) - \frac{1}{2} \eta_h^\alpha \left( \frac{\mu_\star^2}{D} W_h W_{h'} \delta_{\alpha\beta} - \frac{\mu_1^2 \mu_\star^2 \psi_1}{D^2} W_h \lambda_i^\alpha (G_X)_{ii'}^{-1} \lambda_{i'}^\beta W_{h'} + \psi_1 \psi_2 \lambda \delta_{hh'} \right) \eta_{h'}^\beta + i\hat{\lambda}_i^\alpha (\sqrt{P}\lambda_i^\alpha - \eta_h^\alpha \Theta_{hi}) \right)\end{aligned}$$

Note that due to with a slight abuse of notation we got rid of indices  $\mu$ , which all sum up trivially to give a global factor  $N$ .

### C.3.2 Averaging over the deterministic noise

The expectation over the deterministic noise  $W_h$  is a Gaussian integral of the form (32) with:

$$[G_W]_{hh'} = \delta_{hh'} + \frac{\mu_\star^2}{D} \eta_h^\alpha A^{\alpha\beta} \eta_{h'}^\beta, \quad (54)$$

$$[J_W]_h = 0, \quad (55)$$

$$A^{\alpha\beta} = \delta_{\alpha\beta} - \mu_1^2 \psi_1 \frac{1}{D} \sum_{i,j} \lambda_i^\alpha [G_X^{-1}]_{ij} \lambda_j^\beta. \quad (56)$$

Note that the prefactor involves, constant, linear and quadratic terms in  $W$  since:

$$(G_X^{-1} J_X)_i = \frac{\mu_1 \mu_\star \sqrt{\psi_1}}{D} [\eta^\alpha W] [G_X^{-1} \lambda^\alpha]_i.$$

Thus, one obtains:

$$\begin{aligned}\Psi_3^v &= \frac{\psi_2}{D} \int \left( \prod_{\alpha=1}^{2n} d\eta^\alpha d\lambda^\alpha d\hat{\lambda}^\alpha \right) \left( \mu_1^2 \psi_1 \lambda_i^1 \lambda_i^2 + \mu_\star^2 \eta_i^1 \eta_i^2 \right) \left[ \mu_\star^2 [\eta^1 (G_W^{-1}) \eta^2] + \mu_1^2 \psi_1 [\lambda^1 H_W \lambda^2] + 2\mu_1^2 \mu_\star^2 \psi_1 [\lambda^1 S_W \eta^2] \right] \\ &\quad \exp \left( -\frac{n}{2} \log \det(G_X) - \frac{n}{2} \log \det(G_W) - \frac{1}{2} \psi_1 \psi_2 \lambda \sum (\eta_h^\alpha)^2 + i\hat{\lambda}_i^\alpha (\sqrt{P}\lambda_i^\alpha - \eta_h^\alpha \Theta_{hi}) \right),\end{aligned}$$



with

$$(H_W)_{ij} = (G_X^{-1})_{ij} + \frac{\mu_1^2 \mu_\star^2 \psi_1}{D^2} [\eta^\alpha (G_W^{-1}) \eta^\beta] [G_X^{-1} \lambda^\alpha]_i [G_X^{-1} \lambda^\beta]_j, \quad (57)$$

$$(S_W)_{ih} = \frac{1}{D} [G_X^{-1} \lambda^\alpha]_i [G_W^{-1} \eta^\alpha]_h. \quad (58)$$

### C.3.3 Averaging over the random features

The expectation over the random features  $\Theta_{hi}$  is a Gaussian integral of the form (32) with:

$$[G_\Theta]_{hh', ii'} = \delta_{hh', ii'}, \quad (59)$$

$$[J_\Theta]_{hi} = -i \hat{\lambda}_i^\alpha \eta_h^\alpha. \quad (60)$$

Performing this integration results in:

$$\begin{aligned} \Psi_3^v = \frac{\psi_2}{D} \int \left( \prod_{\alpha=1}^{2n} d\eta^\alpha \right) & (\mu_1^2 \psi_1 \lambda_i^1 \lambda_i^2 + \mu_\star^2 \eta_i^1 \eta_i^2) [\mu_\star^2 [\eta^1 (G_W^{-1}) \eta^2] + \mu_1^2 \psi_1 [\lambda^1 H_W \lambda^2] + 2\mu_1^2 \mu_\star^2 \psi_1 [\lambda^1 S_W \eta^2]] \\ & \exp \left( -\frac{n}{2} \log \det(G_X) - \frac{n}{2} \log \det(G_W) - \frac{1}{2} \psi_1 \psi_2 \lambda \sum (\eta_h^\alpha)^2 - \frac{1}{2} \eta_h^\alpha \eta_h^\beta \hat{\lambda}_i^\alpha \hat{\lambda}_i^\beta + i\sqrt{P} \hat{\lambda}_i^\alpha \lambda_i^\alpha \right). \end{aligned}$$

### C.3.4 Expression of the action and the prefactor

To complete the computation we integrate with respect to  $\hat{\lambda}_i^\alpha$ , using again formulae (32):

$$[G_{\hat{\lambda}}]_{ii'}^{\alpha\beta} = \delta^{ii'} \eta_h^\alpha \eta_h^\beta, \quad (61)$$

$$[J_{\hat{\lambda}}]_i^\alpha = i\sqrt{P} \lambda_i^\alpha. \quad (62)$$

This yields the final expression of the term:

$$\begin{aligned} \Psi_3^v = \frac{\psi_2}{D} \int \left( \prod_{\alpha=1}^{2n} d\eta^\alpha \right) \left( \prod_{\alpha=1}^{2n} d\lambda^\alpha \right) & (\mu_1^2 \psi_1 \lambda_i^1 \lambda_i^2 + \mu_\star^2 \eta_i^1 \eta_i^2) [\mu_\star^2 [\eta^1 (G_W^{-1}) \eta^2] + \mu_1^2 \psi_1 [\lambda^1 H_W \lambda^2] + 2\mu_1^2 \mu_\star^2 \psi_1 [\lambda^1 S_W \eta^2]] \\ & \exp \left( -\frac{n}{2} \log \det(G_X) - \frac{n}{2} \log \det(G_W) - \frac{D}{2} \log \det(G_{\hat{\lambda}}) - \frac{1}{2} \psi_1 \psi_2 \lambda \sum (\eta_h^\alpha)^2 - \frac{1}{2} \lambda_i^\alpha (G_{\hat{\lambda}}^{-1})_{ii'}^{\alpha\beta} \lambda_{i'}^\beta \right). \end{aligned}$$

The above may be written as

$$\Psi_3^v = \int \left( \prod d\eta \right) \left( \prod d\lambda \right) P_{\Psi_3^v} [\eta, \lambda] \exp \left( -\frac{D}{2} S^v [\eta, \lambda] \right), \quad (63)$$

with the *prefactor*  $P_{\Psi_3^v}$  and the *action*  $S^v$  defined as:

$$\begin{aligned} P_{\Psi_3^v} [\eta, \lambda] &:= \frac{\psi_2}{D} (\mu_1^2 \psi_1 \lambda_i^1 \lambda_i^2 + \mu_\star^2 \eta_i^1 \eta_i^2) [\mu_\star^2 [\eta^1 (G_W^{-1}) \eta^2] + \mu_1^2 \psi_1 [\lambda^1 H_W \lambda^2] + 2\mu_1^2 \mu_\star^2 \psi_1 [\lambda^1 S_W \eta^2]], \\ S^v [\eta, \lambda] &:= \psi_2 \log \det(G_X) + \psi_2 \log \det(G_W) + \log \det(G_{\hat{\lambda}}) + \frac{1}{D} \psi_1 \psi_2 \lambda \sum (\eta_h^\alpha)^2 + \frac{1}{D} \left( \lambda_i^\alpha (G_{\hat{\lambda}}^{-1})_{ii'}^{\alpha\beta} \lambda_{i'}^\beta \right). \end{aligned}$$

### C.3.5 Expression of the action and the prefactor in terms of order parameters

Here we see that we have a factor  $D \rightarrow \infty$  in the exponential part, which can be estimated using the saddle point method. Before doing so, we introduce the following order parameters:

$$1 = \int dQ_{\alpha\beta} d\hat{Q}_{\alpha\beta} e^{\hat{Q}_{\alpha\beta} (P Q_{\alpha\beta} - \eta_h^\alpha \eta_h^\beta)}, \quad (64)$$

$$1 = \int dR_{\alpha\beta} d\hat{R}_{\alpha\beta} e^{\hat{R}_{\alpha\beta} (D R_{\alpha\beta} - \lambda_i^\alpha \lambda_i^\beta)}. \quad (65)$$

This allows to rewrite the prefactor only in terms of  $Q, R$ : for example,

$$\mu_1^2 \psi_1 \lambda_i^1 \lambda_i^2 + \mu_\star^2 \eta_i^1 \eta_i^2 = \psi_1 D (\mu_1^2 R^{12} + \mu_\star^2 Q^{12}).$$

To do this, there are two key quantities we need to calculate:  $\lambda G_X^{-1} \lambda$  and  $\eta G_W^{-1} \eta$ . To calculate both, we note that  $G_X$  and  $G_W$  are both of the form  $\mathbf{I} + \mathbf{X}$ , therefore their inverse may be calculated using their series representation. The result is:

$$[M_X]^{\alpha\beta} := \frac{1}{D} \lambda^\alpha G_X^{-1} \lambda^\beta = [R(I + \mu_1^2 \psi_1 R)^{-1}]^{\alpha\beta}, \quad (66)$$

$$[M_W]^{\alpha\beta} := \frac{1}{P} \eta^\alpha (G_W^{-1}) \eta^\beta = [Q(I + \mu_1^2 \psi_1 A Q)^{-1}]^{\alpha\beta}. \quad (67)$$

Using the above, we deduce:

$$\lambda^1 H_W \lambda^2 = D M_X^{12} + P \mu_1^2 \mu_\star^2 \psi_1 [M_X M_W M_X]^{12}, \quad (68)$$

$$\lambda^1 S_W \eta^2 = P [M_X M_W]^{12}. \quad (69)$$

The integrals over  $\eta, \lambda$  become simple Gaussian integrals with covariance matrices given by  $\hat{Q}, \hat{R}$ , yielding:

$$1 = \int dQ_{\alpha\beta} d\hat{Q}_{\alpha\beta} e^{-\frac{\psi_1 D}{2} (\log \det \hat{Q} - 2 \text{Tr} Q \hat{Q})}, \quad (70)$$

$$1 = \int dR_{\alpha\beta} d\hat{R}_{\alpha\beta} e^{-\frac{D}{2} (\log \det \hat{R} - 2 \text{Tr} R \hat{R})}. \quad (71)$$

The next step is to take the saddle point with respect to the auxiliary variables  $\hat{Q}$  and  $\hat{R}$  in order to eliminate them:

$$\frac{\partial S^v}{\partial \hat{Q}_{\alpha\beta}} = \psi_1 (\hat{Q}^{-1} - 2Q) = 0 \Rightarrow \hat{Q} = \frac{1}{2} Q^{-1}, \quad (72)$$

$$\frac{\partial S^v}{\partial \hat{R}_{\alpha\beta}} = (\hat{R}^{-1} - 2R) = 0 \Rightarrow \hat{R} = \frac{1}{2} R^{-1}. \quad (73)$$

One finally obtains:

$$\begin{aligned} P_{\Psi_3} [Q, R] &= D \psi_1^2 \psi_2 (\mu_1^2 R^{12} + \mu_\star^2 Q^{12}) \left[ \mu_\star^2 [M_W^v]^{12} + \mu_1^2 \left( M_X^{12} + \mu_1^2 \mu_\star^2 \psi_1^2 [M_X M_W^v M_X]^{12} \right) + 2 \mu_1^2 \mu_\star^2 \psi_1 [M_X M_W^v]^{12} \right], \\ S^v [Q, R] &= \psi_2 \log \det(G_X) + \psi_2 \log \det(G_W) + \psi_1^2 \psi_2 \lambda \text{Tr} Q + \text{Tr} (R Q^{-1}) + (1 - \psi_1) \log \det Q - \log \det R. \end{aligned} \quad (74)$$

### C.3.6 Saddle point equations

The aim is now to use the saddle point method in order to evaluate the integrals over the order parameters. Thus, one looks for  $R$  and  $Q$  solutions to the equations:

$$\frac{\partial S^v}{\partial Q_{\alpha\beta}} = 0, \quad \frac{\partial S^v}{\partial R_{\alpha\beta}} = 0 \quad \forall \alpha, \beta = 1, \dots, 2n.$$

To solve the above, it is common to make a *replica symmetric ansatz*. In this case, we assume that the solutions to the saddle point equations take the form:

$$Q = \begin{bmatrix} q & \tilde{q} & \cdots & \tilde{q} \\ \tilde{q} & \ddots & \ddots & \vdots \\ \vdots & \ddots & \ddots & \tilde{q} \\ \tilde{q} & \cdots & \tilde{q} & q \end{bmatrix}, \quad R = \begin{bmatrix} r & \tilde{r} & \cdots & \tilde{r} \\ \tilde{r} & \ddots & \ddots & \vdots \\ \vdots & \ddots & \ddots & \tilde{r} \\ \tilde{r} & \cdots & \tilde{r} & r \end{bmatrix} \quad (75)$$

The action takes the following form:

$$\begin{aligned} S^v(q, r, \tilde{q}, \tilde{r}) &= 2n (S_0(q, r) + S_1^v(q, r, \tilde{q}, \tilde{r})) \\ S_0(q, r) &= \lambda \psi_1^2 \psi_2 q + \psi_2 \log \left( \frac{\mu_\star^2 \psi_1 q}{\mu_1^2 \psi_1 r + 1} + 1 \right) + \frac{r}{q} + (1 - \psi_1) \log(q) + \psi_2 \log(\mu_1^2 \psi_1 r + 1) - \log(r) \\ S_1^v(q, r, \tilde{q}, \tilde{r}) &= f^v(q, r) \tilde{q} + g^v(q, r) \tilde{r} \\ f^v(q, r) &= \lambda \psi_1^2 \psi_2 + \frac{\mu_\star^2 \psi_1 \psi_2}{\mu_\star^2 \psi_1 q + \mu_1^2 \psi_1 r + 1} + \frac{1 - \psi_1}{q} - \frac{r}{q^2} \\ g^v(q, r) &= -\frac{\mu_\star^2 \mu_1^2 \psi_1^2 \psi_2 q}{(\mu_1^2 \psi_1 r + 1)(\mu_\star^2 \psi_1 q + \mu_1^2 \psi_1 r + 1)} + \frac{\mu_1^2 \psi_1 \psi_2}{\mu_1^2 \psi_1 r + 1} + \frac{1}{q} - \frac{1}{r}. \end{aligned} \quad (76)$$

### C.3.7 Fluctuations around the saddle point

We introduce the following notations:

$$\begin{aligned} [\nabla_{\mathbf{T}} F(\mathbf{T}_\star)]_{\alpha\beta} &= \frac{\partial F}{\partial T_{\alpha\beta}}|_{\mathbf{T}_\star}, \\ [H_{\mathbf{T}} F(\mathbf{T}_\star)]_{\alpha\beta,\gamma\delta} &= \left[ \begin{array}{cc} \frac{\partial^2 F}{\partial Q_{\alpha\beta} \partial Q_{\gamma\delta}} & \frac{\partial^2 F}{\partial Q_{\alpha\beta} \partial R_{\gamma\delta}} \\ \frac{\partial^2 F}{\partial R_{\alpha\beta} \partial Q_{\gamma\delta}} & \frac{\partial^2 F}{\partial R_{\alpha\beta} \partial R_{\gamma\delta}} \end{array} \right] \bigg|_{\mathbf{T}_\star}, \\ H[F] &= \left[ \begin{array}{cccc} \frac{\partial F}{\partial q \partial q} & \frac{\partial F}{\partial q \partial r} & \frac{\partial F}{\partial q \partial \tilde{q}} & \frac{\partial F}{\partial q \partial \tilde{r}} \\ \frac{\partial F}{\partial r \partial q} & \frac{\partial F}{\partial r \partial r} & \frac{\partial F}{\partial r \partial \tilde{q}} & \frac{\partial F}{\partial r \partial \tilde{r}} \\ \frac{\partial F}{\partial \tilde{q} \partial q} & \frac{\partial F}{\partial \tilde{q} \partial r} & \frac{\partial F}{\partial \tilde{q} \partial \tilde{q}} & \frac{\partial F}{\partial \tilde{q} \partial \tilde{r}} \\ \frac{\partial F}{\partial \tilde{r} \partial q} & \frac{\partial F}{\partial \tilde{r} \partial r} & \frac{\partial F}{\partial \tilde{r} \partial \tilde{q}} & \frac{\partial F}{\partial \tilde{r} \partial \tilde{r}} \end{array} \right] \bigg|_{\substack{q=q^* \\ r=r^* \\ \tilde{r}=0 \\ \tilde{q}=0}}. \end{aligned}$$

**Proposition** Let  $q^*$  and  $r^*$  be the solutions of the fixed point equation for the function  $S_0 : (q, r) \mapsto \mathbb{R}$  defined in (76):

$$\begin{cases} \frac{\partial S_0(q, r)}{\partial q} = 0 \\ \frac{\partial S_0(q, r)}{\partial r} = 0. \end{cases}$$

Then we have that

$$\Psi_3^v = \frac{1}{D} \text{Tr} \left[ H[S^v]^{-1} H[P_{\Psi_3^v}] \right]. \quad (77)$$

**Sketch of proof** Solving the saddle point equations:

$$\begin{cases} \frac{\partial S^v(q, r, \tilde{q}, \tilde{r})}{\partial q} = 0 \\ \frac{\partial S^v(q, r, \tilde{q}, \tilde{r})}{\partial r} = 0 \\ \frac{\partial S^v(q, r, \tilde{q}, \tilde{r})}{\partial \tilde{q}} = 0 \\ \frac{\partial S^v(q, r, \tilde{q}, \tilde{r})}{\partial \tilde{r}} = 0 \end{cases},$$

one finds  $\tilde{q} = \tilde{r} = 0$ , which is problematic because the prefactor vanishes:  $P_{\Psi_3} \propto \mu_1^2 \tilde{q} + \mu_\star^2 \tilde{r}$ .

Therefore we must go beyond the saddle point contribution to obtain a non zero result, i.e. we have to examine the quadratic fluctuations around the saddle point. To do so we perform a second-order expansion of the action (74) as a function of  $Q$  and  $R$ :

$$\begin{aligned} P_{\Psi_3^v}(\mathbf{T}) &\approx P_{\Psi_3^v}(\mathbf{T}_\star) + (\mathbf{T} - \mathbf{T}_\star)^\top \nabla P_{\Psi_3^v}(\mathbf{T}_\star) + \frac{1}{2} (\mathbf{T} - \mathbf{T}_\star)^\top H_{\mathbf{T}} [P_{\Psi_3^v}(\mathbf{T}_\star)] (\mathbf{T} - \mathbf{T}_\star), \\ S^v(\mathbf{T}) &\approx S_0(\mathbf{T}_\star) + \frac{1}{2} (\mathbf{T} - \mathbf{T}_\star)^\top H_{\mathbf{T}} [S^v(\mathbf{T}_\star)] (\mathbf{T} - \mathbf{T}_\star). \end{aligned}$$

Computing the second derivative of (74), it is easy to show that:

$$\begin{aligned} [H_{\mathbf{T}} [S^v(\mathbf{T})]]_{\alpha\beta,\gamma\delta} &= [H_{\mathbf{T}} [S^v(\mathbf{T})]]_{\alpha\beta} (\delta_{\alpha\gamma} \delta_{\beta\delta} + \delta_{\alpha\delta} \delta_{\beta\gamma}), \\ [H_{\mathbf{T}} [P_{\Psi_3^v}(\mathbf{T})]]_{\alpha\beta,\gamma\delta} &= [H_{\mathbf{T}} [P_{\Psi_3^v}(\mathbf{T})]]_{\alpha\beta} (\delta_{\alpha\gamma} \delta_{\beta\delta} + \delta_{\alpha\delta} \delta_{\beta\gamma}), \end{aligned}$$

where

$$\begin{aligned} H_{\mathbf{T}} [F]_{\alpha\beta} &= \left[ \begin{array}{cc} \frac{\partial^2 F}{\partial Q_{\alpha\beta} \partial Q_{\alpha\beta}} & \frac{\partial^2 F}{\partial Q_{\alpha\beta} \partial R_{\alpha\beta}} \\ \frac{\partial^2 F}{\partial R_{\alpha\beta} \partial Q_{\alpha\beta}} & \frac{\partial^2 F}{\partial R_{\alpha\beta} \partial R_{\alpha\beta}} \end{array} \right] \\ &= \frac{1}{2n} \delta_{\alpha\beta} \left[ \begin{array}{cc} \frac{\partial^2 F}{\partial q \partial q} & \frac{\partial^2 F}{\partial q \partial r} \\ \frac{\partial^2 F}{\partial r \partial q} & \frac{\partial^2 F}{\partial r \partial r} \end{array} \right] + \frac{2}{2n(2n-1)} (1 - \delta_{\alpha\beta}) \left[ \begin{array}{cc} \frac{\partial^2 F}{\partial \tilde{q} \partial \tilde{q}} & \frac{\partial^2 F}{\partial \tilde{q} \partial \tilde{r}} \\ \frac{\partial^2 F}{\partial \tilde{r} \partial \tilde{q}} & \frac{\partial^2 F}{\partial \tilde{r} \partial \tilde{r}} \end{array} \right]. \end{aligned}$$

Hence,

$$\begin{aligned}
\Psi_3^v &= \lim_{n \rightarrow 0} \int d\mathbf{T} P_{\Psi_3^v}(\mathbf{T}) \exp^{-\frac{D}{2} S^v(\mathbf{T})}, \\
&= \lim_{n \rightarrow 0} \underbrace{P_{\Psi_3^v}(\mathbf{T}_\star)}_0 + \nabla P_{\Psi_3^v}(\mathbf{T}_\star)_{\alpha\beta} \underbrace{\int d\mathbf{T} (\mathbf{T} - \mathbf{T}_\star)_{\alpha\beta} \exp\left(-\frac{D}{2} S^v(\mathbf{T})\right)}_0 \\
&\quad + \frac{1}{2} H_{\mathbf{T}} [P_{\Psi_3^v}(\mathbf{T}_\star)]_{\alpha\beta} \int d\mathbf{T} (\mathbf{T} - \mathbf{T}_\star)_{\alpha\beta}^2 \exp\left(-\frac{D}{2} S^v(\mathbf{T})\right) \\
&= \lim_{n \rightarrow 0} \frac{1}{2} H_{\mathbf{T}} [P_{\Psi_3^v}(\mathbf{T}_\star)]_{\alpha\beta} e^{-\frac{D}{2} S^v(\mathbf{T}_\star)} \int d\mathbf{T} (\mathbf{T} - \mathbf{T}_\star)_{\alpha\beta}^2 e^{-\frac{D}{2} \sum_{\alpha\beta} (\mathbf{T} - \mathbf{T}_\star)_{\alpha\beta}^2} H_{\mathbf{T}} [S^v(\mathbf{T}_\star)]_{\alpha\beta} \\
&= \lim_{n \rightarrow 0} \frac{1}{2} \frac{(2\pi)^n}{\det H_{\mathbf{T}} [S^v(\mathbf{T}_\star)]} e^{-\frac{D}{2} S^v(\mathbf{T}_\star)} \frac{2}{D} H_{\mathbf{T}} [P_{\Psi_3^v}(\mathbf{T}_\star)]_{\alpha\beta} H_{\mathbf{T}} [S^v(\mathbf{T}_\star)]_{\alpha\beta}^{-1} \\
&= \frac{1}{D} \text{Tr} \left[ H [S^v]^{-1} H [P_{\Psi_3^v}] \right]
\end{aligned}$$

In the last step, we used the fact that:

$$\begin{aligned}
\lim_{n \rightarrow 0} e^{-\frac{D}{2} S^v(\mathbf{T}_\star)} &= \lim_{n \rightarrow 0} e^{-n D S_0(q_\star, r_\star)} = 1, \\
\lim_{n \rightarrow 0} \det H_{\mathbf{T}} [S^v(\mathbf{T}_\star)] &= 1.
\end{aligned}$$

The last equality follows from the fact that for a matrix of size  $n \times n$  of the form  $M_{\alpha\beta} = a\delta_{\alpha\beta} + b(1 - \delta_{\alpha\beta})$ , we have

$$\det M = (a - b)^n \left( 1 + \frac{nb}{a - b} \right) \xrightarrow{n \rightarrow 0} 1.$$

### C.3.8 Expression of the vanilla terms

Using the above procedure, one can compute the terms  $\Psi_1, \Psi_2^v, \Psi_3^v$  of (49): for each of these terms, the action is the same as in (74), and the prefactors can be obtained as:

$$\begin{aligned}
P_{\Psi_1}[Q, R] &= \mu_1^2 \psi_1 \psi_2 \left( M_X^{11} + \mu_1^2 \mu_\star^2 \psi_1^2 (M_X M_W M_X)^{11} + \mu_\star^2 \mu_1 \psi_1 (M_X M_W)^{11} \right), \\
P_{\Psi_2^v}[Q, R] &= D \psi_1^2 \psi_2 (\mu_1^2 R^{12} + \mu_\star^2 Q^{12}) (\mu_1^2 \psi_2 P_{XX} - 2\mu_1^2 \mu_\star^2 \psi_1 \psi_2 P_{XW} + \mu_\star^2 P_{WW}), \\
P_{\Psi_3^v}[Q, R] &= D \psi_1^2 \psi_2 (\mu_1^2 R^{12} + \mu_\star^2 Q^{12}) \left[ \mu_\star^2 [M_W^v]^{12} + \mu_1^2 \left( M_X^{12} + \mu_1^2 \mu_\star^2 \psi_1^2 [M_X M_W^v M_X]^{12} \right) + 2\mu_1^2 \mu_\star^2 \psi_1 [M_X M_W^v]^{12} \right], \\
P_{XX} &= N_X^{12} + \frac{1}{\psi_2} M_X^{12} + 2(\mu_1 \mu_\star \psi_1)^2 [N_X M_W M_X]^{12} + \frac{(\mu_1 \mu_\star \psi_1)^2}{\psi_2} [M_X M_W M_X]^{12} + (\mu_1 \mu_\star \psi_1)^4 [M_X M_W N_X M_W M_X]^{12}, \\
P_{XW} &= [N_X M_W]^{12} + \frac{1}{\psi_2} [M_X M_W]^{12} + (\mu_1 \mu_\star \psi_1)^2 [M_X M_W N_X M_W]^{12}, \\
P_{WW} &= M_W^{12} + \psi_2 (\mu_1 \mu_\star \psi_1)^2 [M_W N_X M_W]^{12}.
\end{aligned}$$

Where a new term appears:

$$[N_X]^{\alpha\beta} = [R(I + \mu_1^2 \psi_1 R)^{-2}]^{\alpha\beta}. \quad (78)$$

## C.4 Computation of the *ensembling* terms

### C.4.1 Expression of the action and the prefactor

In the *ensembling* terms, the two inverse matrices are different, hence one has to introduce two distinct replica variables. We distinguish them by the use of an extra index  $a \in \{1, 2\}$ , denoted in brackets in order not to be confused with the replica indices  $\alpha$ .

$$\left[ M^{(1)} \right]_{ij}^{-1} \left[ M^{(2)} \right]_{kl}^{-1} = \lim_{n \rightarrow 0} \int \left( \prod_{\alpha=1}^n \prod_{a=1}^2 d\eta^{\alpha(a)} \right) \eta_i^{1(1)} \eta_j^{1(1)} \eta_k^{1(2)} \eta_l^{1(2)} \exp \left( -\frac{1}{2} \sum_{(a)} \eta^{\alpha(a)} M_{ij}^{(a)} \eta^{\alpha(a)} \right). \quad (79)$$

Calculations of the Gaussian integrals follow through in a very similar way as for the *vanilla* terms. The matrices appearing in the process are:

$$(G_X^e)_{ii'} = \delta_{ii'} + \frac{\mu_1^2 \psi_1}{D} \sum_{(a)\alpha} \lambda_i^{\alpha(a)} \lambda_{i'}^{\alpha(a)}, \quad (80)$$

$$(J_X^e)_i = \frac{\mu_1 \mu_* \sqrt{\psi_1}}{D^2} \sum_{\alpha a} \lambda_i^{\alpha(a)} \eta_h^{\alpha(a)} W_h^{(a)}, \quad (81)$$

$$(G_W^e)_{hh'}^{(ab)} = \delta_{hh'}^{ab} + \frac{\mu_*^2}{D} \sum_{\alpha\beta} \eta_h^{\alpha(a)} A_e^{\alpha\beta,ab} \eta_{h'}^{\beta(b)}, \quad (82)$$

$$(J_W^e)_h = 0 \quad (83)$$

$$(G_\Theta^e)_{hh',ii'}^{(ab)} = \delta_{hh',ii'}^{ab} \quad (84)$$

$$(J_\Theta^e)_{hi}^{(a)} = -i \sum_{\alpha} \hat{\lambda}_i^{\alpha(a)} \eta_h^{\alpha(a)}, \quad (85)$$

$$(G_{\hat{\lambda}}^e)_{ii'}^{\alpha\beta,(ab)} = 2\delta^{ab} \delta^{ii'} \eta_h^{\alpha(a)} \eta_h^{\beta(b)}, \quad (86)$$

$$(J_{\hat{\lambda}}^e)_i^{\alpha(a)} = i\sqrt{P} \lambda_i^{\alpha(a)}. \quad (87)$$

$$(88)$$

with

$$A_e^{\alpha\beta,(ab)} = \delta_{ab} \delta_{\alpha\beta} - \mu_1^2 \psi_1 \frac{1}{D} \sum_{i,j} \lambda_i^{\alpha(a)} [G_X^{e-1}]_{ij} \lambda_j^{\beta(b)}, \quad (89)$$

$$[H_W^e]_{ii'} = [G_X^{e-1}]_{ii'} + \sum_{\alpha\beta,ab} \left[ G_X^{e-1} \lambda^{\alpha(a)} \right]_i \left[ G_X^{e-1} \lambda^{\beta(b)} \right]_{i'} \left[ \eta^{\alpha(a)} [G_W^{e-1}]^{(ab)} \eta^{\beta(b)} \right], \quad (90)$$

$$[S_W^e]_{ih} = \frac{1}{D} \sum_{\alpha,a} \left[ G_X^{e-1} \lambda^{\alpha(a)} \right]_i \left[ G_W^{e-1} \eta^{\alpha(a)} \right]_h. \quad (91)$$

Starting with the computation of  $\Psi_3^e$  in order to illustrate the method used, the prefactor  $P_{\Psi_3^e}$  and the action are  $S^e$  are given by:

$$P_{\Psi_3^e}[\eta, \lambda] := \frac{\mu_1^2 \psi_1 \psi_2}{D} \lambda_i^{1(1)} \lambda_i^{1(2)} \left[ \mu_*^2 \left[ \eta^{1(1)} (G_W^{e-1})^{(12)} \eta^{1(2)} \right] + \mu_1^2 \psi_1 \left[ \lambda^{1(1)} H_W^e \lambda^{1(2)} \right] + 2\mu_1^2 \mu_*^2 \psi_1 [\lambda^{1(1)} S_W^e \eta^{1(2)}] \right], \quad (92)$$

$$S^e[\eta, \lambda] := \psi_2 \log \det(G_X^e) + \psi_2 \log \det(G_W^e) + \log \det(G_{\hat{\lambda}}^e) + \frac{1}{D} \psi_1 \psi_2 \lambda \sum (\eta_h^{\alpha(a)})^2 + \frac{1}{2D} \left( \lambda_i^{\alpha(a)} (G_{\hat{\lambda}}^{e-1})_{ii'}^{\alpha\beta,ab} \lambda_{i'}^{\beta(b)} \right). \quad (93)$$

#### C.4.2 Expression of the action and the prefactor in terms of order parameters

This time, because of the two different systems, the order parameters carry an additional index  $a$ , which turns them into  $2 \times 2$  block matrices:

$$1 = \int dQ_{\alpha\beta}^{(ab)} d\hat{Q}_{\alpha\beta}^{(ab)} e^{\hat{Q}_{\alpha\beta}^{(ab)} (PQ_{\alpha\beta}^{(ab)} - \eta_h^{\alpha(a)} \eta_h^{\beta(b)})}, \quad (94)$$

$$1 = \int dR_{\alpha\beta}^{(ab)} d\hat{R}_{\alpha\beta}^{(ab)} e^{\hat{R}_{\alpha\beta}^{(ab)} (dR_{\alpha\beta}^{(ab)} - \lambda_i^{\alpha(a)} \lambda_i^{\beta(b)})}. \quad (95)$$

The systems being decoupled, we make the following ansatz for the order parameters:

$$Q = \left[ \begin{array}{ccc|ccc} q & \cdots & 0 & \tilde{q} & \cdots & 0 \\ \vdots & \ddots & \vdots & \vdots & \ddots & \vdots \\ 0 & \cdots & q & 0 & \cdots & \tilde{q} \\ \hline \tilde{q} & \cdots & 0 & q & \cdots & 0 \\ \vdots & \ddots & \vdots & \vdots & \ddots & \vdots \\ 0 & \cdots & \tilde{q} & 0 & \cdots & q \end{array} \right], \quad R = \left[ \begin{array}{ccc|ccc} r & \cdots & 0 & \tilde{r} & \cdots & 0 \\ \vdots & \ddots & \vdots & \vdots & \ddots & \vdots \\ 0 & \cdots & r & 0 & \cdots & \tilde{r} \\ \hline \tilde{r} & \cdots & 0 & r & \cdots & 0 \\ \vdots & \ddots & \vdots & \vdots & \ddots & \vdots \\ 0 & \cdots & \tilde{r} & 0 & \cdots & r \end{array} \right]. \quad (96)$$

In virtue of the simple structure of the above matrices, the replica indices  $\alpha$  trivialize and we may replace the matrices  $Q$  and  $R$  by the  $2 \times 2$  matrices:

$$Q = \begin{bmatrix} q & \tilde{q} \\ \tilde{q} & q \end{bmatrix}, \quad R = \begin{bmatrix} r & \tilde{r} \\ \tilde{r} & r \end{bmatrix}.$$

Define:

$$[M_X^e]_{(ab)} \equiv \frac{1}{D} \lambda_i^{(a)} [G_X^{e-1}]_{ij} \lambda_j^{(b)} = [R(I + \mu_1^2 \psi_1 R)^{-1}]_{(ab)}, \quad (97)$$

$$[M_W^e]_{(ab)} \equiv \frac{1}{P} \eta^{(a)} [G_W^{e-1}]^{(ab)} \eta^{(b)} = [Q(I + \psi_1 A^e Q)^{-1}]_{(ab)}, \quad (98)$$

where products are now over  $2 \times 2$  matrices. Then, one has:

$$\begin{aligned} P_{\Psi_3^e}[Q, R] &:= D \mu_1^2 \psi_1^2 \psi_2 R^{(12)} \left[ \mu_\star^2 M_W^{e(12)} + \mu_1^2 \left( M_X^{e(12)} + \mu_1^2 \mu_\star^2 \psi_1^2 [M_X^e M_W^e M_X^e]^{(12)} \right) + 2 \mu_1^2 \mu_\star^2 \psi_1 [M_X^e M_W^e]^{(12)} \right], \\ S^e[Q, R] &:= \psi_2 \log \det(G_X^e) + \psi_2 \log \det(G_W^e) + \sum_a \left[ (\psi_1^2 \psi_2 \lambda) \text{Tr} Q^{(a)(a)} + \text{Tr} \left( R^{(a)(a)} (Q^{-1})^{(a)(a)} \right) + \log \det Q^{(a)(a)} \right] \\ &\quad - \psi_1 \log \det Q - \log \det R. \end{aligned}$$

Where we have:

$$M_X^e = \frac{1}{(1 + \mu_1^2 \psi_1 r)^2 - (\mu_1^2 \psi_1 \tilde{r})^2} \begin{bmatrix} r + \mu_1^2 \psi_1 (r^2 - \tilde{r}^2) & \tilde{r} \\ \tilde{r} & r + \mu_1^2 \psi_1 (r^2 - \tilde{r}^2) \end{bmatrix}, \quad (99)$$

$$A_{(ab)}^e = \delta_{(ab)} - \mu_1^2 \psi_1 [M_X^e]_{(ab)}, \quad (100)$$

$$[M_W^e]_{(ab)} = q \delta_{(ab)} - \mu_\star^2 \psi_1 [A^e (I + \mu_\star^2 \psi_1 q A^e)^{-1}]_{(ab)}, \quad (101)$$

$$\det(G_X^e) = \det(\delta_{(ab)} + \psi_1 \mu_1^2 R_{(ab)}), \quad (102)$$

$$\det(G_W^e) = \det(\delta_{ab} + \psi_1 q A_{(ab)}^e). \quad (103)$$

Finally, we are left with:

$$\begin{aligned} S^e(q, r, \tilde{q}, \tilde{r}) &= n (S_0(q, r) + S_1^e(q, r, \tilde{q}, \tilde{r})), \\ S_1^e(q, r, \tilde{q}, \tilde{r}) &= \tilde{r}^2 f^e(q, r) + \tilde{q}^2 g^e(q, r), \\ f^e(q, r) &= \frac{2r \mu_1^2 \psi_1 (1 + q \mu_\star^2 \psi_1) + (1 + q \mu_\star^2 \psi_1)^2 - r^2 \mu_1^4 \psi_1^2 (-1 + \psi_2)}{2r^2 (1 + r \mu_1^2 \psi_1 + q \mu_\star^2 \psi_1)^2}, \\ g^e(q, r) &= \frac{\psi_1}{2q^2}. \end{aligned}$$

Where  $S_0$  was defined in (76).

### C.4.3 Expression of the ensembling terms

Evaluating the fluctuations around the saddle point follows through in the same way as for the vanilla terms, with the following expressions of the prefactors:

$$P_{\Psi_2^e}[Q, R] = D \psi_1^2 \psi_2 \mu_1^2 \tilde{r} [\mu_1^2 P_{XX}^e - 2 \mu_1^2 \mu_\star^2 \psi_1 P_{WX}^e + \mu_\star^2 P_{WW}^e], \quad (104)$$

$$P_{\Psi_3^e}[Q, R] = D \mu_1^2 \psi_1^2 \psi_2 R^{(12)} \left[ \mu_\star^2 M_W^{e(12)} + \mu_1^2 \left( M_X^{e(12)} + \mu_1^2 \mu_\star^2 \psi_1^2 [M_X^e M_W^e M_X^e]^{(12)} \right) + 2 \mu_1^2 \mu_\star^2 \psi_1 [M_X^e M_W^e]^{(12)} \right], \quad (105)$$

$$\begin{aligned} P_{XX}^e &= \psi_2 N_X^{e12} + M_X^{e12} + 2 \psi_2 (\mu_1 \mu_\star \psi_1)^2 [M_X^e N_X^e M_W^e]^{12} + (\mu_1 \mu_\star \psi_1)^2 [M_X^e M_W^e M_X^e]^{12} \\ &\quad + \psi_2 (\mu_1 \mu_\star \psi_1)^4 [M_X^e M_W^e N_X^e M_W^e M_X^e]^{12}, \end{aligned} \quad (106)$$

$$P_{WX}^e = \psi_2 [N_X^e M_W^e]^{12} + [M_X^e M_W^e]^{12} + \psi_2 (\mu_1 \mu_\star \psi_1)^2 [M_X^e M_W^e N_X^e M_W^e]^{12}, \quad (107)$$

$$P_{WW}^e = [M_W^e]^{12} + \psi_2 (\mu_1 \mu_\star \psi_1)^2 [M_W^e N_X^e M_W^e]^{12}. \quad (108)$$

## C.5 Computation of the *divide and conquer* term

Here, we are interested in computing the term  $\Psi_2^d$ . This term differs from the previous ones in that there are now two independent data matrices  $\mathbf{X}^{(1)}$  and  $\mathbf{X}^{(2)}$ . The calculations for the action and the prefactor are very similar to calculations performed for the *ensembling* terms  $\Psi_2^e, \Psi_3^e$ , with the addition that  $\mathbf{X}$  now also carries an index  $(a)$ .

Firstly let us write  $\Psi_2^d$  as a trace over random matrices:

$$\Psi_2^d = \frac{\mu_1^2}{d^2} \text{Tr} \left[ \mathbf{X}^{(1)} \mathbf{Z}^{(1)} \mathbf{B}^{(1)-1} \boldsymbol{\Theta}^{(1)} \boldsymbol{\Theta}^{(2)} \mathbf{B}^{(2)-1} \mathbf{Z}^{(2)} \mathbf{X}^{(2)} \right]. \quad (109)$$

Calculations follow through in the same way as in the previous sections. Using the replica formula (79), and performing the integrals over the Gaussian variables the following quantities appear:

$$(G_X^d)_{ii'}^{(ab)} = \delta_{ii'} + \frac{\mu_1^2 \psi_1}{D} \sum_{\alpha} \lambda_i^{\alpha(a)} \lambda_{i'}^{\alpha(a)}, \quad (110)$$

$$(J_X^d)_i^{(a)} = \frac{\mu_1 \mu_{\star} \sqrt{\psi_1}}{D^2} \sum_{\alpha} \lambda_i^{\alpha(a)} \eta_h^{\alpha(a)} W_h^{(a)}, \quad (111)$$

$$(G_W^d)_{hh'}^{(ab)} = \delta_{hh'}^{ab} + \frac{\mu_{\star}^2}{D} \sum_{\alpha\beta} \eta_h^{\alpha(a)} A^{\alpha\beta, ab} \eta_{h'}^{\beta(b)}, \quad (112)$$

$$(J_W^d)_h = 0, \quad (113)$$

$$(G_{\Theta}^d)_{hh', ii'}^{(ab)} = \delta_{hh', ii'}^{ab}, \quad (114)$$

$$(J_{\Theta}^d)_{hi}^{(a)} = -i \sum_{\alpha} \hat{\lambda}_i^{\alpha(a)} \eta_h^{\alpha(a)}, \quad (115)$$

$$(G_{\lambda}^d)_{ii'}^{\alpha\beta, (ab)} = 2\delta^{ab} \delta^{ii'} \eta_h^{\alpha(a)} \eta_h^{\beta(b)}, \quad (116)$$

$$(J_{\lambda}^d)_i^{\alpha(a)} = i\sqrt{P} \lambda_i^{\alpha(a)}. \quad (117)$$

$$(118)$$

The saddle point ansatz for  $Q$  and  $R$  is the same as the one for the ensembling terms (see (96)). The procedure to evaluate  $\Psi_2^d$  is also the same as the one for  $\Psi_2^e$  except the Hessian is taken with respect to  $S^d$ . The final result is given below.

$$\begin{aligned} P_{\Psi_2^d}[Q, R] &= D \mu_1^2 \psi_1 \psi_2^2 \tilde{r} \left[ \psi_1 \mu_1^2 P_{XX} + 2 \mu_{\star}^2 \mu_1^2 \psi_1^2 P_{WX} + \mu_{\star}^2 \psi_1 P_{WW} \right], \\ P_{XX} &= \left( N_X^{11} + 2(\mu_1 \mu_{\star} \psi_1)^2 [N_X M_W M_X]^{11} + (\mu_1 \mu_{\star} \psi_1)^4 [M_X M_W N_X M_W M_X]^{11} \right), \\ P_{WX} &= [N_X M_W]^{11} + (\mu_1 \mu_{\star} \psi_1)^2 [M_X M_W N_X M_W]^{11}, \\ P_{WW} &= (\mu_1 \mu_{\star} \psi_1)^2 [M_W N_X M_W]^{11}, \\ S^d[q, r, \tilde{q}, \tilde{r}] &= n \left( S_0(q, r) + S_1^d(q, r, \tilde{q}, \tilde{r}) \right), \\ S_1^d(q, r, \tilde{q}, \tilde{r}) &= \frac{\tilde{r}^2}{r^2} + \frac{\psi_1 \tilde{q}^2}{q^2}. \end{aligned}$$

With:

$$\begin{aligned} M_X &= \frac{r}{1 + \mu_1^2 \psi_1 r}, \\ A &= 1 - \mu_1^2 \psi_1 M_X, \\ M_W &= \frac{q}{1 + \mu_{\star}^2 \psi_1 q A}, \\ N_X &= \frac{\tilde{r}}{(1 + \mu_1^2 \psi_1 r)^2}. \end{aligned}$$